Highly-resolved satellite remote sensing based land-use change inventory yields weaker surface albedo-induced global cooling

Authors: Xiaohu Jian[1], Xiaodong Zhang[1,*], Xinrui Liu[1], Kaijie Chen[1], Tao Huang[2], Shu Tao[1], Junfeng Liu[1], Hong Gao[2], Yuan Zhao[2], Ruiyu Zhugu[1], Jianmin Ma[1]

Affiliations:

[1]Laboratory for Earth Surface Processes, College of Urban and Environmental Sciences, Peking University, Beijing 100871, PR China

[2] Key[2]Key Laboratory for Environmental Pollution Prediction and Control, Gansu Province, College of Earth and Environmental Sciences, Lanzhou University, Lanzhou 730000, PR China

*Corresponding author:** Xiaodong Zhang (zhangxd2020@pku.edu.cn)

Abstract

Land-use change (LUC) is ranked as the second anthropogenic source of climate change after fossil fuel burning and yields negative albedo-induced radiative forcing (ARF). This cooling effect has been assessed using low spatiotemporally resolved LUC datasets derived from historical statistical data with large uncertainties. Herein, we implement a satellite remote sensing derived highly resolved LUC dataset into a compact earth system model and reassess the global and regional surface ARF by LUC from 1983 to 2010 relative to 1750. We find that the magnitude of negative ARF obtained from the present study is lower by 20% than that estimated by the Intergovernmental Panel on Climate Change, implying a weaker cooling effect. The result reveals that the global LUC-induced surface albedo change may not significantly slow down global warming as was previously anticipated. Sub-Saharan Africa made the largest net contributionproportion to the magnitude of global ARF (39.2%), due to substantial land use conversions, typically the conversion from forest to other vegetation lands, which accompany with higher surface albedos. The most remarkable land cover changes occurred in East and Southeast Asia, which dominated the changes in global ARF in recent

30 decades. Based on major land cover types in these two regions, we infer that vegetation lands

31 exert a most vital effect on global ARF variation.

1. Introduction

34   Anthropological activities that have effectuated global climate change can be primarily

35 categorized under greenhouse gas emissions, the emissions of aerosols, and land use change

36 (LUC) (IPCC AR6, 2021). LUC in different temporal and spatial scales varies rapidly from

37 local to global scales, with significant ramifications for the climate system, and is one of the

38 key drivers of global climate change (Feddema et al., 2005; Cai et al., 2004; Foley et al., 2005;

39 Houghton et al., 2012; Zhu et al., 2019). LUC accounts for 13%–20% of the total anthropogenic

40 carbon emissions from the 1990s to the 2010s, and 20% in the 1980s and 1990s (Houghton et

41 al., 2012), ranking as the second source of anthropogenic climate change after fossil fuel

42 combustion (Andrews et al., 2017). The influence of LUC on climate change is primarily

43 manifested in two critical processes: the radiation/energy interface between the surface and the

44 atmosphere and the changes in the carbon source/sink. LUC affects climate by emitting or

45 absorbing greenhouse gases in the atmosphere, modifying the carbon cycle within the climate

46 system. In other words, the effect of LUC on climate balance involved in understanding how

47 changes in land use (such as afforestation, urbanization, or land restoration) affect the climate

48 system's energy balance through biogeochemical and biogeophysical processes. These

49 processes drive carbon sequestration and emissions and surface albedo change (Gries et al.,

50 2019). LUC also modifies the albedo and roughness of the underlying surface, altering the

51 surface heat budget. By functioning as a carbon sink through carbon reduction-oriented land

52 management, LUC plays a pivotal role in the sequestration of carbon (IPCC AR6, 2021). Such

53 LUC-induced carbon sinks are crucial for compensating emissions from other carbon sources,

54 such as fossil fuel energy, transportation, and housing, that continue to emit carbon dioxide.

55   The extent of the influence of LUC on the climate system and energy balance is often

56 measured in terms of radiative forcing (RF) (Andrews et al., 2017; Andrews et al., 2020;

57 Ramanathan et al., 1975; Bonan et al., 2008; Betts et al., 2000; Ward et al., 2014). The primary

effect of RF on climate change is through a temperature feedback mechanism (Sherwood et al., 2015). While the effects of LUC on climate balance have been extensively studied from the biogeochemical perspective (Foley et al., 2005; Houghton et al., 2012; Vose et al., 2004; Gries et al., 2019), knowledge gaps still remain in the understanding of LUC-induced climate forcing. from the biogeophysical perspective. This is partly due to the lack of extensive investigations in the long-term effects of LUC-induced climate forcing prediction and uncertainties in this field (IPCC AR6, 2021). Immediate impacts may be different from those observed over decades or centuries. Long-term temporal studies that track these changes are limited. The commonly held belief is that the change in surface albedo associated with LUC has a negative forcing globally, leading to a cooling effect and functioning as a carbon sink. However, the magnitudes of negative forcing vary between -0.15 W m^{-2} and -0.6 W m^{-2} in different studies spanning the pre-industrial to industrial era (IPCC AR3, 2001; Myhre et al., 2003; Hansen et al., 2004; Betts et al., 2007; Forster et al., 2007; Pongratz et al., 2009; Ward et al., 2014; Li et al., 2016; Jiao et al., 2017). The Intergovernmental Panel on Climate Change (IPCC) AR3 report (2001) (IPCC AR3, 2001) adopted -0.25 ± 0.25 W m^{-2} as the global average RF due to surface albedo change. This value has been revised in subsequent reports to -0.15 ± 0.10 W m^{-2} (IPCC AR6, 2021). The magnitude of negative RF induced by surface albedo (hereafter referred to as ARF) obtained from other studies appears to be greater than the IPCC adopted value (Fig. 1). In AR3 of the IPCC, the scientific understanding of LUC-induced ARF was deemed "very low". Due to the limited number of studies and the uncertainty of historical land cover (LC) changes, IPCC AR6 (2021) assigns these values a medium confidence level. A substantial proportion of the uncertainties in LUC and ARF can be attributed to the lack of high spatiotemporal resolution in LUC data and sufficient supports by measurements (Gong et al., 2013; Winkler et al., 2021; Jian et al., 2022). Recently, numerous high-resolution remote sensing datasets have been used to develop highly resolved LUC datasets (Gong et al., 2013; Winkler et al., 2021). Modern satellites are equipped with sensors that offer high spatial resolution, allowing for the detailed mapping of land-use changes. This level of detail is essential for identifying specific types of land-use changes, such as deforestation, urban expansion, or agricultural intensification, each of which has different impacts on radiative

87 forcing. These remote sensing-based datasets reveal that LUC has affected as much as one-
88 third of the world's land area in just six decades (1960–2019), roughly four times greater than
89 the estimates from long-term land change assessments conducted previously (Winkler et al.,
90 2021). It is interesting to know if and to what extent recently developed remote sensing-based
91 global land use (LU) change data with very high spatial-temporal resolution from a climate
92 perspective and potentially low uncertainty could improve the estimation of LUC-induced
93 global and regional climate forcing.

94 In the present study, we reassessed the LUC forced ARF by incorporating a high-
95 resolution (5 km×5 km) satellite remote sensing measured LUC dataset into a compact earth
96 system model (see Methods) and evaluate the contributions from various LUC and LU types
97 in different regions/countries to global ARF, aiming to provide a more precise and
98 measurement-based estimate of regional and global ARF.
99

2. Materials and Methods

2.1. OSCAR Model

102 OSCAR v2.4 (Gasser et al., 2017), a compact model of global biogeochemical cycles, is
103 used to investigate the effect of LUC-induced changes in surface albedo on global RF. OSCAR
104 is not spatially resolved but country and region-based. It is a nonlinear box model incorporating
105 as many key climate components and modules as possible, such as LU change and aerosol
106 physics-chemistry feedback. The model was designed to simulate long-term trends in earth
107 system change rather than seasonal and interannual variations in the earth system. OSCAR is
108 also a parametric model in which several parameters required to calculate RF are calibrated on
109 (or input from) complex climate models. Model uncertainties are assessed by Monte Carlo
110 ensembles, including input LUC, surface albedo, and other model parameters. In the present
111 study, we have assigned a 5% uncertainty in OSCAR modeled ARF based on LUC data
112 uncertainty. The uncertainty of the LUC data is subject to its accuracy (82.81%, Liu et al.,
113 2020). We examined the response of modeled ARF to the 5% uncertainty by increasing the
114 uncertainty to 10% and 15%. The differences of simulated mean ARF between 5% and 10%

and 15% were only 0.23% and 0.47%, respectively. Further details, advantages of OSCAR model, and the motivations to use OSCAR model in our ARF simulations are presented in Supplementary Text 1.

2.2. Updated Global LUC Data

The OSCAR's capability to simulate LU change-induced RF is one of its strengths. To assess the combined effects of human activities on the carbon-climate system (Hurtt et al., 2011), the model employs the LU Harmonization (LUH1) LUC dataset developed under IPCC-AR5. The results show a smooth transition of annual changes in LUC, suggesting that approach and data sources adopted to derive LUH1 (Supplementary Text 2) likely missed some important characteristics of LU transitions, resulting in a substantial uncertainty in the modeled LUC-induced RF. Although LUH1 was recently updated to LUH2 with a spatial resolution of $0.25° \times 0.25°$ latitude/longitude (Hurtt et al., 2020), in the present study, we chose the Global Land Surface Satellite-Global LC dataset (GLASS-GLC) (Liu et al., 2020) to replace the LUH1 inventory with coarse spatial resolution in the OSCAR model to capture the temporal-spatial variations of LUC adequately. GLASS-GLC was developed using 5 km×5 km resolution GLASS (Global Land Surface Satellite) climate data records from 1982 to 2015. Although both LUH and GLASS-GLC provide annual LUC, compared to previous LUC products, such as LUH1 and LUH2, GLASS-GLC based on satellite remote sensing has greater consistency, a higher spatial resolution, and many LU types. Compared to LUH1 dataset derived based on historical statistics and census data combining with the History Database of the Global Environment (HYDE) model and the Global Land-use Model (GLM) (Hurtt et al., 2011), the GLASS-GLC dataset uses the Google Earth Engine (GEE) platform with the latest version of GLASS CDRs (climate data records) from 1982 to 2015 (Liu et al., 2020) to obtain a more reliable land use inventory.

It should recognize the differences between the satellite-derived land cover classifications (GLASS-LUC) and the land use classifications (LUH1) and reconcile the differences. Table S1 list mapping categories of the LUH1 and GLASS-GLC. GLASS-GLC considers seven LUC

classes, including cropland, forest, grassland, shrubland, tundra, barren land, and snow/ice, with an overall accuracy of 82.81%. Although the GLASS-GLC data source also include urban areas, these small areas are not straightforward to be distinguished at the 5 km×5 km resolution as compared to other LUCs (Liu et al., 2020). ~~Although~~Besides, while urban expansion could contribute to climate warming (Ouyang et al., 2022), our previous work (Jian et al., 2022) has explored the impact of urbanization on China's ARF and found that the impact of urban sprawl on China's ARF is very small (0.59%) and hence can be neglected, although China has experienced the world's most rapid urbanization since the 1980s~~,~~ (Yang et al., 2013), due to considerably smaller area of urban land than the other selected 6 LU categories. Likewise, the urban land also exerts a little effect on ARF from a global perspective. Therefore, urban areas were not taken into consideration in this study. The LUC data are available for download at https://doi.org/10.1594/PANGAEA.913496. Noted that, although the updated GLASS-GLC was extended to 2015, given that some of parameters and variables in OSCAR v2.4 were only available up to 2010, we performed OSCAR simulations from 1982 to 2010.

We further compared the GLASS-LUC derived ARF in the OSCAR model to the modeling result using another satellite remote sensing derived LUC, namely, the MODIS LUC data (Moderate Resolution Imaging Spectroradiometer, 2014, https://modis.gsfc.nasa.gov/). Given that the MODIS-LUC data is only available from 2001 to 2023, we replaced the GLASS-GLC by MODIS LUC data from 2002 to 2010 in the OSCAR model. During this period, the accumulated RF simulated by the OSCAR in the globe using the MODIS LULC and the GLASS-GLC data are 0.0165 Wm^{-2} and 0.0157 $W\ m^{-2}$, respectively, indicating only a 5% difference of between the RFs using the two LUC datasets derived from satellite remote sensing. Sun et al. (2022) compared the applications of six LULC products in the identification of LUCs in Northwestern China. Their results revealed, while the GLASS-GLC and MODIS (MCD-12Q1) were not superior to other four products, these two datasets were of most temporal and spatial consistency.

The OSCAR model does not take the surface roughness length into account. The surface roughness affects primarily on turbulent exchange of heat and air mass between the underlying

surface and air, which may indirectly alter surface radiation fluxes via changing sensible and latent fluxes under a heat balance status (Andrews, 2012). ~~Since~~This characteristic can significantly influence RF largely via its association with surface albedo. Given that the OSCAR ~~model does not consider~~introduces directly the surface albedo, it is expected that excluding the roughness length~~, the impact of LUC on surface roughness is not included in the present study~~. would not perturbate RF prediction significantly.

2.3. Sensitivity Analysis

To illustrate the influence of LUC-induced albedo change on the global RF, we chose five LU types that have dominated the global LUCs over the past four decades: cropland, desert, forest, grassland, and shrub. ~~We~~Considering that, for many satellite-derived land-use classification products, overall classification accuracies range between 70% and 90%, implying that misclassifications can lead to an uncertainty of 10% to 30% in land-use area estimates (Gong et al., 2013), we carried out extensive sensitivity experiments by reducing each LU transition area by 20% within five major LU types (cropland, desert, forest, grassland, and shrub~~), aiming~~). These sensitivity evaluations aimed to examine the relative significance and contribution the LU conversion and transition among different LU types to the ARF. Among them, each LU type is converted to the rest four LU types, thereby accounting for total 20 LU transitions and sensitivity experiments. However, in the original OSCAR inventory, there were only inter-conversions between cropland and other land types, and no conversions between desert, forest, grassland, and shrub. Table ~~S1~~S2 presents these 20 LU transitions from 1982 to 2010. To facilitate analysis and refine the effect of LUC on ARF, the world has been divided into nine regions. These regions include East and Southeast Asia (including China), Europe, Latin America, the Near East and North Africa, North America, Oceania, Russia, Sub-Saharan Africa, and South Asia (Fig. 2). Table ~~S2~~S3 presents the surface albedos for the five LU types in each nation and the nine regrouped global regions. Between the OSCAR LUH1-LUC inventory and the GLASS-GLC inventory, Fig. S1 and Table ~~S3~~S4 compare annual changes in the area of each LU type from 1982 to 2010 in the globe and the nine regions. There

199 are distinct differences between the two LUC inventories. The causes of these differences and

200 two simulation results are discussed in Supplementary Text 2. By performing OSCAR

201 simulations with a low spatiotemporally resolved OSCAR LUH1-LUC inventory (Scenario 1)

202 and a high spatiotemporally resolved GLASS-GLC inventory (Scenario 2), respectively, we

203 also set up two model scenarios for sensitivity experiments. Detailed results of sensitivity

204 analysis are presented in Table S5

205

2.4 Methods of comparing ARF results for two datasets

207 The percentage changes in annual ARF between the two scenarios are estimated using the

208 following equation:

209 $ARF_F = (ARF_{S2} - ARF_{S1}) \times 100\% / ARF_{S1}$ (1)

210 where ARF_F, ARF_{S1}, and ARF_{S2} represent the percentage changes in ARF and ARF values from

211 model scenarios 1 and 2, respectively.

212

2.5. Disturbance Capacity Analysis and Effective Area

214 We conducted comprehensive sensitivity experiments on OSACR simulations to analyze

215 the impact of each of the 20 LU conversions on ARF globally and across of the nine regions.

216 We consider the conversion from each of the five LU types to the remaining four LU types,

217 resulting in 20 LU conversion types (Table ~~S1~~S2). In these sensitivity experiments, we

218 introduce a disturbance capacity (DC, %) that determines the magnitude of the ARF change

219 induced by the 20 LU conversions in the region of interest. The DC is defined as follows:

220
$$
\begin{cases}
\Delta RF_{ij} = \overline{RF_i} - \overline{RF'_{ij}}, \\
\\
DC_{ij} = \dfrac{\Delta RF_{ij}}{\sum_{j=1}^{20} |\Delta RF_{ij}|} * 100\%.
\end{cases}
\tag{2}
$$

221 where, $\overline{RF_i}$ represents mean ARF in region i averaged from 1983 to 2010. We reduce the jth

222 LU conversion in region i by 20% and define resulted ARF in region i as RF'_{ij} in each year.

223 Its mean from 1983 to 2010 is defined as $\overline{RF'_{ij}}$. Expression (2) can also be considered as a

224   statistical formula for determining the relative significance or the contribution of ARF induced

225   by a particular LU conversion to the total ARF change across all regions and LU conversion

226   types. For example, the sensitivity experiment for grassland to cropland conversion in region i

227   (13th sensitivity experiment or LU conversion) was conducted by multiplying the area

228   converted from grassland to cropland by 0.8, indicating a 20% reduction in the grassland to the

229   cropland transition area. The changes (or response) of ARF in region i perturbed by a 20%

230   reduction in the jth LU conversion area ΔRF_{ij} were then used to estimate DC_{ij} (Eq. 2).

231   We also examine net LU conversion among the five LU types, where net LU conversion

232   is defined as the difference between a pair of LU conversions. For instance, the net conversion

233   from grassland to cropland (13th LU conversion, Table ~~S1~~S2) and from cropland to grassland

234   (3rd LU conversion, Table ~~S1~~S2) is calculated as the area converted from grassland to cropland

235   minus the area converted from cropland to grassland, also referred to as the net two-way

236   conversion. This adjustment reduces the total LU conversions in the sensitivity experiment

237   from 20 to 10. The DC for the ten net LU conversion areas is definable as follows:

238
$$
\begin{cases}
A_{a \leftrightarrow b}^{t} = A_{a \rightarrow b}^{t} - A_{b \rightarrow a}^{t}, \\[2mm]
DC_{a \leftrightarrow b} = \frac{DC_{a \rightarrow b}}{|DC_{a \rightarrow b}|} * \left(\frac{|DC_{a \rightarrow b}| + |DC_{b \rightarrow a}|}{2} \right).
\end{cases}
\tag{3}
$$

239   where $A_{a \leftrightarrow b}^{t}$ is the area of net LU transition, a and b indicate the conversion from LU type a

240   to type b, respectively, $A_{a \rightarrow b}^{t}$ and $A_{b \rightarrow a}^{t}$ are the transition areas from LU type a to LU type b,

241   and from LU type b to a. The superscript t denotes a specific year between 1982 and 2010.

242   $DC_{a \leftrightarrow b}$ represents the disturbance capacity of net conversion between paired LUs, and $DC_{a \rightarrow b}$

243   and $DC_{b \rightarrow a}$ are the DC of LU conversion $a \rightarrow b$ and $b \rightarrow a$, respectively. After the DC of LU

244   conversion is determined, we estimate an effective area (EA) (see main text), which is defined

245   here as the cumulative area of six net LU conversions, given by

$$\begin{cases} \alpha_{ik} = \dfrac{DC_{ik}}{\sum |DC_{ik}|}, if\ |DC_{ik}| \geq 1\%, \\[2em] \alpha_{ik} = 0, if\ |DC_{ik}| < 1\%, \\[2em] A^e_{it} = \sum_{k=1}^{10} \alpha_{ik} * A_{ikt}. \end{cases} \qquad (4)$$

246

where DC_{ik} represents the DC in the *kth* net LU conversion type affecting ARF in region *i*. The ratio of DC_{ik} to the absolute value of total DC_{ik}, defined by in Eq. (4), can also be viewed as the proportion of different net LU conversions to the global EA (Table S4S6). A^e_{it} denotes the EA in year *t* and region *i*. A^e_{it} indicates the area of the *kth* net LU conversion type in year *t* and region *i*. Consequently, the EA measures the extent of a LU conversion area that significantly impacts the change in ARF. In calculating the EA, we first exclude net LU conversions with |DC| > 1%, then sum up these |DC| values (Σ|DC|) and finally divide the DC of each net LU conversion with |DC| > 1% by Σ|DC| (Eq. 4). Table S4S6 presents the correlation coefficients and significance tests of the EAs. According to Eq. 4, once the DC is obtained, the EA area can be estimated, which defines the converting areas of the 10 net land conversion types between 1982 and 2010 divided by their respective absolute DCs. The results explain the change in ARF from 1983 to 2010 (Supplementary Text 3).

2.6. Quantifying the Contribution of Regional LU Transition to Changes in Global ARF and Effective Area

The changes in ARF due to LU conversion in a region from 1983 to 2010 can be simply defined as the differences in ARF between 1983 and 2010. First, we considered the ARF change in any region across the globe as:

$$\Delta ARF_{LU\_all} = RF'^{\,2010}_i - RF'^{\,1983}_i. \qquad (5)$$

where, $RF'^{\,2010}_i$ and $RF'^{\,1983}_i$ denote the ARF in *the ith* region in the S2 scenario using the GLASS-GLC inventory in 2010 and 1983, respectively. To remove the effect of LU conversion on ARF, we reduced the transition area of each LU type from 20% to 100% in the 20 sensitivity

269 experiments, meaning no occurrence of LU transition. Second, we introduced

270 $RF_{i,j}^{2010}$ and $RF_{i,j}^{1983}$ to represent the ARF in the ith region induced by the jth LU transition in

271 the S2 scenario in 2010 and 1983, so their differences are as follows:

272 $$\Delta ARF_{LU\_ind} = RF_{i,j}^{2010} - RF_{i,j}^{1983}. \tag{6}$$

273 This can be regarded as the changes in ARF induced by other 19 conversion types for the jth

274 LU conversion during this period. The changes in ARF subject to any LU conversion in any of

275 the nine regions can be written as:

276 $$\delta_F = \Delta ARF_{LU\_all} - \Delta ARF_{LU\_ind}. \tag{7}$$

277 In other words, δ_F indicates the net effect of regional LU transition on ARF. Finally, the

278 contribution of ARF from any region and any LU conversion to the changes in global ARF is

279 defined as:

280 $$C_{ARF} = \frac{\delta_f}{ARF_{global}^{2010} - ARF_{global}^{1983}}. \tag{8}$$

281 here, ARF_{global}^{2010} and ARF_{global}^{1983} are global ARF in 2010 and 1983 from model scenario 2.

282 Their difference is constant (0.0364 W m^{-2}).

283   The contribution of regional EAs to the global EA is simply estimated by Eq. 9:

284 $$C_{EA} = \alpha_{i,k} \times \frac{\sum_{n=1}^{28} \frac{EA_{n,i}}{\sum_i^9 EA_{n,i}}}{28}. \tag{9}$$

285 where, $i = 1, 2, \ldots 9$ denotes nine regions, $n = 1, 2, \ldots 28$ is the number of years from 1983 to

286 2010 and $\alpha_{i,k}$ is defined in Eq. (4).

287   The contribution of two-way LU conversions to the changes in global ARF is defined by

288 Eq. 10:

289 $$C_{LV}^k = \sum_{i=1}^{9} \sum_{j=1}^{8} C_{ARF}^{i,j}. \tag{10}$$

where, $k = 1,2…5$ denotes five LU types, $i = 1, 2,…,9$ denotes nine regions, and $j = 1,2,…,8$ indicate paired two-way LU transitions. Taking cropland as an example, the one-way transitions between cropland to the remaining four LU types are the transitions from cropland to forestland, grassland, desert, and shrubland. The other way includes transitions from forestland, grassland, desert, and shrubland to cropland. So the two-way transition includes eight LU conversions.

3. Results

3.1. Response of Global RF to Perturbed Albedo
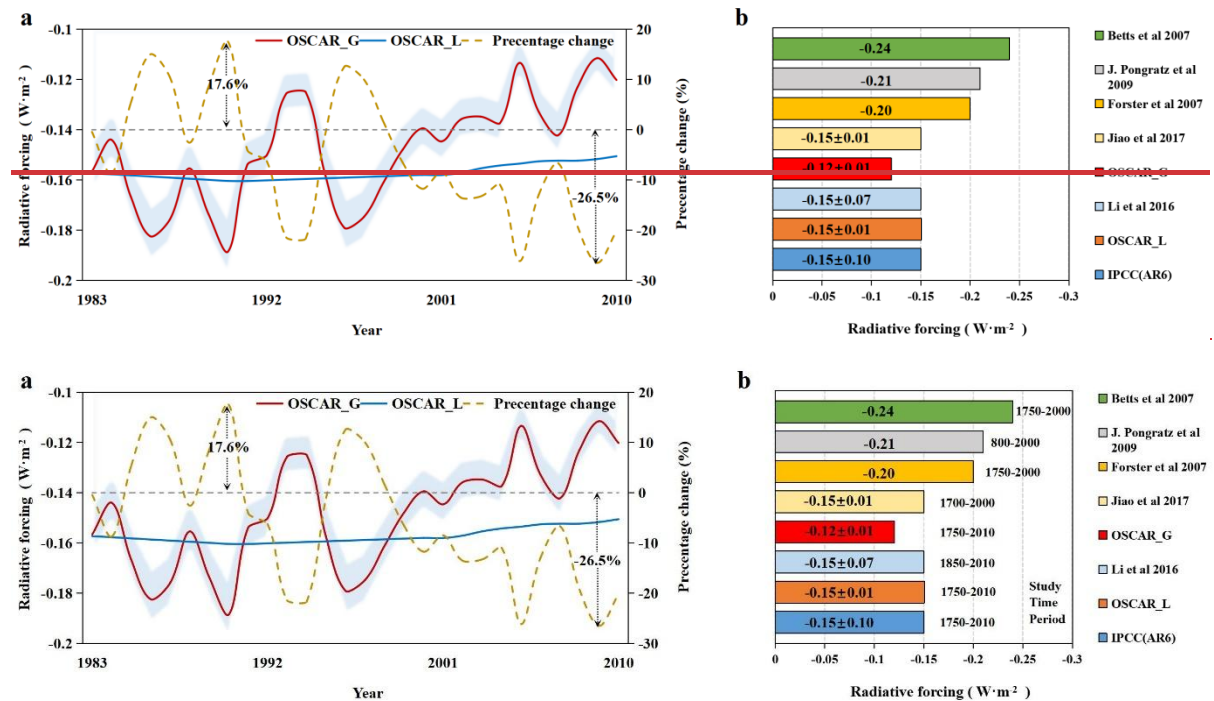
Figure 1. Annual RF (W m^{-2}) due to albedo change and ARF percentage change (%) and different ARF derived from previous studies. (a) OSCAR-modeled annual RF due to the albedo change and ARF percentage change between the two model scenarios S1 and S2 from 1983 to 2010 derived from coarse resolution LUH1-LUC inventory (solid blue line, see 'Methods') and GLASS-GLC inventory (solid red line, see Methods). The annual ARF of 1983 through 2010 from both model scenarios is relative to the baseline year of 1750. Two-tailed T-Test yields a p-value of 0.025 (<0.05), indicating the statically significant difference between OSCAR-G and OSCAR-L data series. Pale blue shading indicates the uncertainty

308 interval estimated from Monte Carlo simulations. Dashed yellow line stands for a percentage change in ARF

309 from the two scenarios. (b) ARF from present (red color bar) and previous (other color bars) studies from

310 ~~the industrial era to~~different time period. However, the results of the studies covering the year 2010 all point

311 to the result of 2010.

312

313   To examine the extent of the changes in global RF subject to the altered surface albedo

314 derived from LU transition from 1983 to 2010, we compared the ARF using the coarse

315 resolution LU Harmonization v1-LU Change [LUH1-LUC inventory (OSCAR_L, model

316 scenario S1)] extending from 1750 to 2010 and the fine resolution Global Land Surface

317 Satellite-Global LC dataset [GLASS-GLC inventory (OSCAR_G, model scenario S2)] in

318 OSCAR simulations. It is noted that the annual ARF derived from the model scenario 1 was

319 relative to the baseline year of 1750. The annual ARF derived from the model scenario 2 was

320 also relative to 1750 but we replaced LUH1-LUC with GLASS-GLC after 1982. Fig. 1a depicts

321 the OSCAR-simulated annual global ARF subject to the two model scenarios. From 1983 to

322 2010, annual ARFs derived from the two LUC scenarios demonstrated upward trend. In

323 contrast, the ARF in the S1 simulation (solid blue line) displays a smoother variation and a

324 weaker increase with a linear trend of 0.0003 (P-value < 0.01). The smooth transition from

325 historical LUC estimates to future projections in the LUH1-LUC results in such gradual

326 changes in the ARF. In contrast, the ARF in the S2 simulation (solid red line) displays strong

327 interannual fluctuations and a more rapid increase with a linear trend of 0.0018 (P-value $<$

328 0.01). The dashed brown line indicates the resulting ARF_F ranges from -26.5% (2009) to 17.6%

329 (1990). Globally, both scenarios produce negative forcing, consistent with previous estimates

330 (IPCC AR6, 2021; Li et al., 2016). As aforementioned, even though we only replaced the

331 coarse resolution LUH1-LUC inventory with the fine resolution GLASS-GLC inventory, the

332 ARF in the OSCAR is predicted since the industrialization era in the 1750s, the same as the

333 IPCC AR6. This suggests that both scenario simulations utilized the same LUH1-LUC data

334 before 1982. Consequently, significant annual and decadal changes in ARF have occurred over

335 the past few decades, alongside rapid and remarkable global variations in LUC. The significant

336 differences in the ARF between the two scenarios can be attributed to different data sources

and approaches applied to derive LUH1-LUC and GLASS-GLC. The former was developed from a combination of historical statistics, population census data, HYDE, and GLM models. Because the time covered by this inventory are outside the period of satellite observations, large uncertainties in LUH1-LUC have been recognized (Hurtt et al., 2020). A higher resolution land use dataset can ensure interannual consistency and comparability of the LUC, and enables the accurate estimation of the rate and mode in LUC (Gong et al., 2013; Liu et al., 2020), which can capture more detailed LUC and LU transitions. Recent reports indicate that the global LUC is four times larger than previously estimated (Winkler et al., 2021). The differences between the two LUC datasets are shown in Supplementary Text 2, Text 4, Table S3S4, and Fig. S1.

Previously estimated global ARF with coarse resolution LUC data has been subject to several concerns. According to the IPCC Assessment Reports, the global RF induced by LUC from pre-industrial times to the present due to changes in land albedo is approximately -0.15 ± 0.10 W m^{-2}, indicating that ARF plays a cooling role (IPCC AR6, 2021). Considering that radiative forcing is often accumulated from the past, the differences of ARF from the two inventories occurred mostly in final year, namely 2010. Our OSCAR simulation under scenario 1 using a LUH1-LUC inventory yielded the same negative ARF value of -0.15 W m^{-2} as reported by the IPCC (Fig. 1b). Using coarse resolution and historical statistics-based LUC data, additional studies have also obtained ARF results with great uncertainties. As depicted in Fig. 1b, all previous studies yielded stronger negative ARFs than the IPCC's estimate, with the negative ARF reaching as low as -0.24 W m^{-2} (Betts et al., 2007). However, our estimation subject to scenario 2 yields an ARF of -0.12 ± 0.01 W m^{-2}, which is only half of that reported by Betts et al (2007). The result suggests that the global LUC-induced surface albedo change may not be acting as anticipated to slow down the global warming.

3.2. Contribution of Regional LUC to Global ARF

364
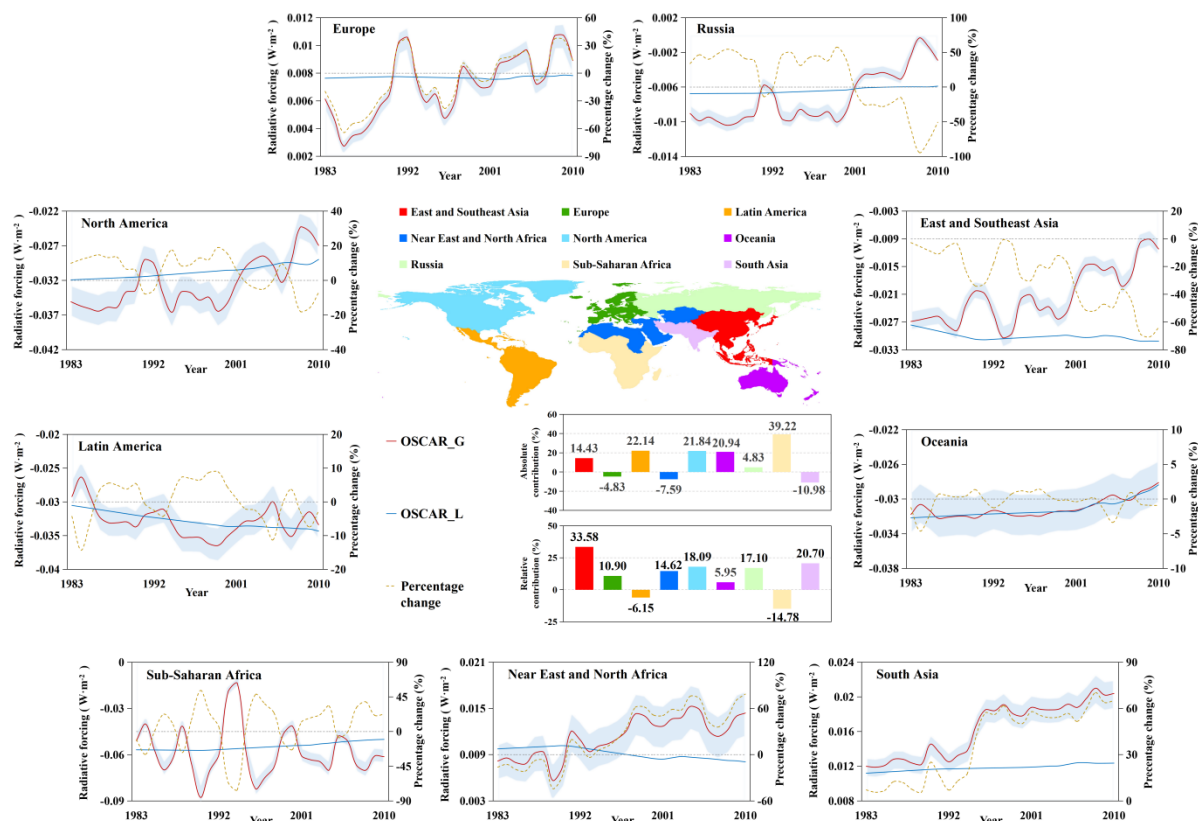
Figure 2. Annual RF (W m^{-2}) due to the albedo change and ARF percentage change between the two model scenarios S1 and S2 from 1983 to 2010 derived from LUH1-LUC inventory (solid blue line) and GLASS-GLC inventory (solid red line) in nine regions across the globe. The pale blue shading indicates the uncertainty interval estimated from Monte Carlo simulations. The dashed brown line stands for the percentage change in the annual ARF$_{i-F}$ between the LUH1-LUC inventory (ARF$_{i-S1}$) and GLASS-GLC inventory (ARF$_{i-S2}$), in which i represents regions, respectively, including East and Southeast Asia, Europe, Latin America, Near East and North Africa, North America, Oceania, Russia, Sub-Saharan Africa, and South Asia. The first bar chart illustrates the absolute contribution of different regions to the global albedo-induced RF, and the second bar chart displays the relative contribution of different regions to the global albedo-induced RF changes. The nine color bars represent different regions, as indicated by the color legend above the colored sectional map.

376

377   In recent decades, LUC has been subject to significant spatial heterogeneity across the
378   globe. To investigate the magnitude of the response of global ARF to continental/regional LUC

since the 1980s, we divided 113 countries and ~~regions in OSCAR into nine regions. These~~ ~~include East and Southeast Asia, Europe, Latin America, the Near East and North Africa, North~~ ~~America, Oceania, Russia, Sub-Saharan Africa, and South Asia (see Table S2).~~territories in OSCAR into nine regions. Each of the nine regions encompasses a specific number of countries and territories (Table S3). The mean ARF value for each of the nine regions was calculated by averaging the ARFs over the countries and territories in each of the nine regions. The colored sectional map in the center of Fig. 2 indicates the nine regions. In addition, the annual variation of the ARF subjected to GLASS-GLC (W m^{-2}, solid red line, scaled on the left Y-axis) and its percentage change (%, dashed brown line, scaled on the right Y-axis) in each of these regions are illustrated in the nine-line charts of Fig. 2. Below the sectional map are two bar charts depicting the absolute and relative contributions of the nine regions to the global ARF. Correspondingly, the total contribution is defined as the proportion of the mean ARF of each nine regions to the global mean ARF from 1983 to 2010. The relative contribution is defined as the proportion of the change in ARF in each of the nine regions to the change in global ARF between 1983 and 2010. In addition, the OSCAR-simulated ARFs in each region derived from LUH1-LUC (solid blue line, scaled to the left on the Y-axis) are displayed in the line charts. Herein, OSCAR predicts ARFs by incorporating fine-scale variations, as opposed to the LUH1-LUC-derived ARFs with smoothing variations; GLASS-GLC, on the other hand, displays more pronounced annual fluctuations. In East and Southeast Asia and Near East and North Africa, the simulated ARFs derived from the two LUC datasets exhibit opposite trends from 1983 to 2010, indicating that LUC data substantially influence regional and continental ARFs.

As evident from the bar charts below the sectional map, among the nine regions, Sub-Saharan Africa, with a mean ARF of −0.06 W m^{-2} on average from 1983 to 2010, made the largest net contribution (39.2%) to the global mean ARF. The significant contribution from Sub-Saharan Africa is attributable to its large desert area of 697.37 Mha with a high albedo (Table ~~S2~~S3) and pronounced LU conversions among vegetated LU types (Fig. S2 and Table ~~S3~~S4). South Asia had a mean ARF of 0.02 W m^{-2} from 1983 to 2010. This region had an absolute negative contribution of −10.98% to the global mean ARF averaged over the nine regions, most likely because of rapidly expanding croplands (226.93 Mha) with low albedo

408 associated with the Green Revolution (Pingali et al., 2012; Liu et al., 2021; Huang et al., 2022)

409 (Fig. S2 and Table S3S4). East and Southeast Asia, Europe, Latin America, Near East and

410 North Africa, North America, Oceania, and Russia contributed 14.43%, −4.83%, 22.14%,

411 −7.59%, 21.84%, 20.94%, and 4.83% to the global mean ARF, respectively.

412 Although East and Southeast Asia made a moderate absolute contribution to the global

413 mean ARF compared to other regions, this region experienced the largest LU change between

414 1982 and 2010. This was characterized by the highest ARF change ($0.017 \ \mathrm{W \ m^{-2}}$), comprising

415 the most significant relative contribution (33.58%) to the global ARF change. Such a

416 contribution can be attributed to the massive LC changes brought on by afforestation and the

417 management of land desertification during this time period (Liu & Xin, 2021; Imai et al., 2018;

418 Zhang et al., 2016), which led to a decrease in surface albedo. In contrast, deforestation in Sub-

419 Saharan Africa in recent decades (Keenan et al., 2015) promoted rapid shrub growth (Atsri et

420 al., 2018; Mograbi et al., 2015), resulting in a rise in albedo. Consequently, this region has the

421 largest negative contribution to the global ARF change, at −14.78%, promoting a cooling effect

422 on the global climate. Similarly, the deforestation in Latin America caused by the conversion

423 of forest to cropland and pastureland in recent decades (Armenteras et al., 2021; Hansen et al.,

424 2013; Nogueira et al., 2019; Davidson et al., 2012) also led to the increase in surface albedo,

425 thus, contributing −6.15% to the global ARF change between 1983 and 2010.

426 The differences (percentage change, %) in regional ARF between the two scenarios for

427 the nine regions are depicted by the brown dashed lines (scaled on the right Y-axis) in the line

428 charts of Fig. 2. Except for Europe, the Near East and North Africa, and South Asia, where the

429 annual ARFs are stronger than those derived from LUH1-LUC, the percentage changes in most

430 regions exhibit the opposite phase of the ARFs predicted by OSCAR using GLASS-GLC. In

431 East and Southeast Asia, for instance, the ARF derived from the S1 model scenario decreased

432 from $-0.028 \ \mathrm{W \ m^{-2}}$ in 1983 to $-0.031 \ \mathrm{W \ m^{-2}}$ in 2010, indicating a reinforced cooling effect.

433 In contrast, the ARF derived from the S2 scenario using the GLASS-GLC inventory exhibits

434 the change from $-0.027 \ \mathrm{W \ m^{-2}}$ in 1983 to $-0.011 \ \mathrm{W \ m^{-2}}$ in 2010, indicating an attenuated

435 cooling effect. The result suggests again that the LUH1-LUC inventory does not capture the

436 change in LUC in East and Southeast Asia since the 1980s. Other details are presented in Table

437 ~~S5~~S7. Similar variations and trends of GLASS-GLC-driven ARFs can be observed in Russia,

438 North America, and Oceania, where the negative ARFs exhibit rising trends from 1983 to 2010,

439 indicating once again the declining negative ARF values and weakening cooling effect. In

440 South Asia, the average percentage change in ARF between the two scenarios is the highest, at

441 37.30%. Moreover, Europe, the Near East and North Africa, and South Asia yielded positive

442 ARFs. The increasing ARF trends indicate an intensification of the warming effect in these

443 regions during this period. Sub-Saharan Africa experienced the greatest negative ARF values

444 and fluctuations in both model scenarios. We found that the ARF from the S1 scenario extended

445 from -0.057 W m^{-2} in 1983 to -0.050 W m^{-2} in 2010. The ARF from the S2 scenario dropped

446 from -0.051 W m^{-2} in 1983 to -0.061 W m^{-2} in 2010. These results illustrate that the LUH1-

447 LUC data attenuates the cooling effect in Sub-Saharan Africa, whereas the GLASS-GLC

448 inventory enhances the cooling effect, demonstrating once again that the LUC data with

449 significantly different resolutions and sources could alter the conclusions in the evaluation of

450 LUC-induced climate forcing. Further details are provided in Supplementary Text 4 and Table

451 ~~S5~~S7.

452

453 **3.3. Effective Area of LU Conversion and Interannual ARF Variations**

454

455
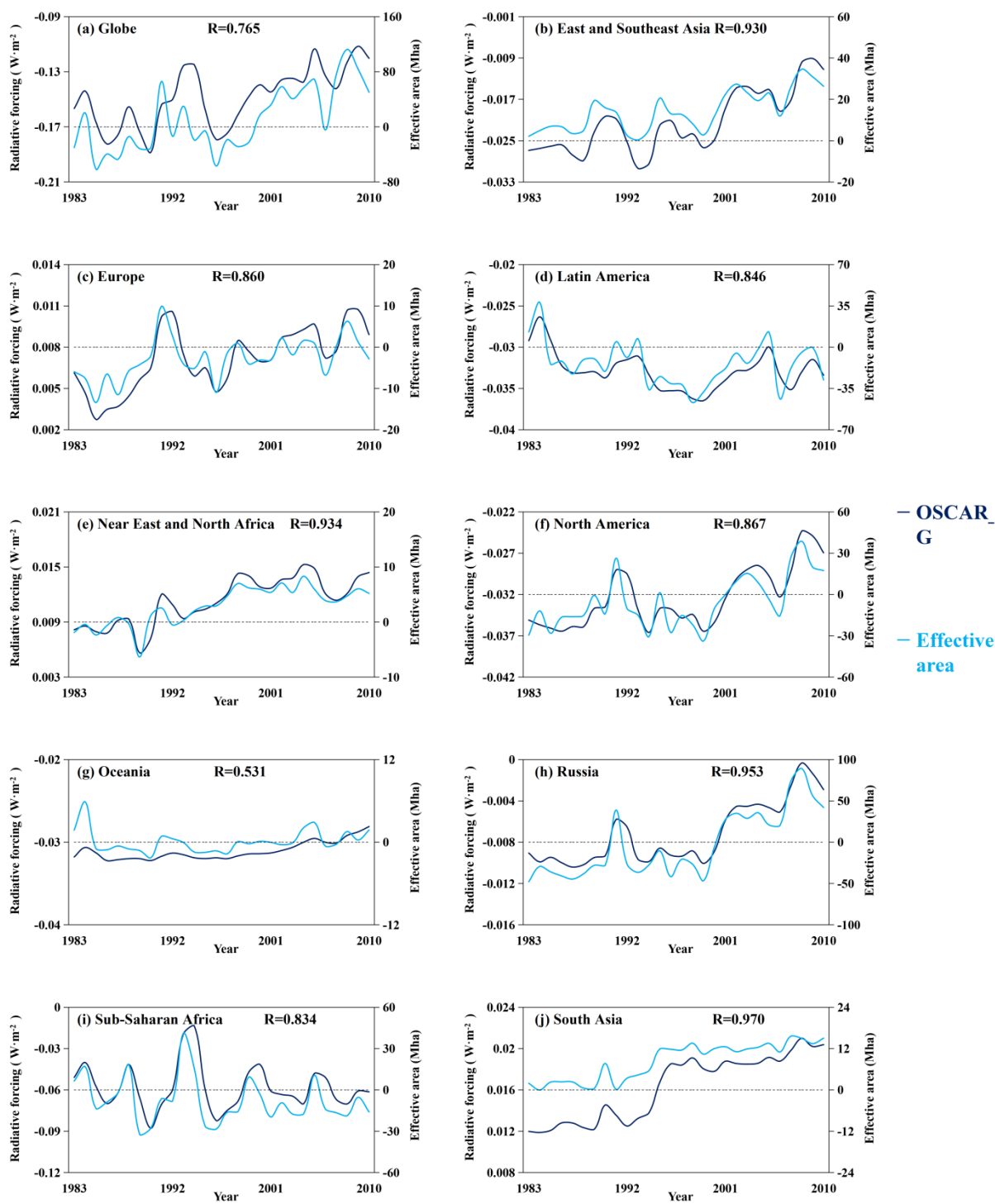
Figure 3. Annual RF (W m^{-2}) due to surface albedo change in model scenarios 2 from 1983 to 2010 derived

from GLASS-GLC inventory (solid black line) and effective area (solid blue line) in the globe and nine

458   regions. (a) Globe; (b) East and Southeast Asia; (c) Europe; (d) Latin America; (e) Near East and North

459   Africa; (f) North America; (g) Oceania; (h) Russia; (i) Sub-Saharan Africa; (j) South Asia. Correlation

460   coefficients between the ARF and effective area are marked in the figures. The effective area measures the

461   extent of the area of all net LU conversion contributing to the change in ARF (see Methods).

462

463   We designed 20 sensitivity experiments to examine the contribution of LU conversion

464   among the five LU types to the variation in ARF from 1982 to 2010 (Methods, Table ~~S1~~S2).

465   We introduced a disturbance capacity (DC, %), and an effective area (EA, see Eq. 4 in Methods)

466   to explain the changes in ARF caused by the size of LU conversion areas. Here, DC (%)

467   quantifies the extent of LU conversion that may considerably impact the change in ARF. The

468   EA is the sum of six net LU conversions that quantifies the extent of LU conversion

469   contributing to the change in ARF. In the sensitivity experiments, we reduced the area of LU

470   transition by 20% for each LU conversion (Gong et al., 2013). The model combines the ARF

471   results from 20 sensitivity experiments with the LUC for each target region. Further details are

472   provided in Methods and Supplementary Text 3. We also analyzed the rate and magnitude of

473   annual ARF fluctuations associated with EAs in the world and nine regions between 1983 and

474   2010. The details are presented in Supplementary Text 5 and Figs. S3–S12.

475   Figure 3 depicts the annual ARF (scaled on the left Y-axis) and EA (scaled on the right

476   Y-axis) in the globe and nine selected regions. As seen, the global annual ARF, which is the

477   sum of the ARFs in the nine regions based on OSCAR simulations, is stronger than regional

478   ARF due to the larger scale of global land cover change (Table ~~S3~~S4 and Fig. S1) and stronger

479   albedo changes. The correlation coefficient between the ARF and EA in the globe is 0.765 (*P*-

480   value < 0.01), indicating that the net LU conversion area in the globe explains 59% of the

481   global ARF variation. In this instance, the global EA consists of a cumulative area of six net

482   LU conversion types. The percentage of individual LU conversions to the global EA is

483   presented in Table ~~S4~~S6 and Fig. S13. As shown in Fig. S13a, the interannual fluctuations of

484   the EA (blue solid line) agree well with that of the transition area from the grassland-to-forest

485   land (red dashed line). Together with the grassland to cropland transition, these two LU

486   transitions contribute the most to the global LU transition, accounting for 52.5% of the total

487   EA worldwide. Such significant LU conversions have been attributed to grassland degradation

488   (Bardgett et al., 2021; Andrade et al., 2015; Aune et al., 2018; Berangere et al., 2018), such as

489   the expansion of croplands in the US, which reduced prairie grasslands (Lark et al., 2020).

490   Since the surface albedo of grassland is greater than that of forest and cropland (Edouard et al.,

491   2010; Jackson et al., 2008), grassland degradation could be considered a major contributor to

492   the increase in global ARF since the mid-1990s (Fig. 3a). This increasing ARF is crucial to the

493   attenuation of the cooling effect of the global negative ARF from -0.15 W m^{-2} to -0.12 W m^{-2}.

494   In East and Southeast Asia, the correlation coefficient between ARF and EA is 0.930 (P-value

495   < 0.01), indicating that the EA explains 86% of the ARF change in this region. In particular,

496   the interannual fluctuation of the EA agree well with the LU transition from cropland to

497   forestland (green dashed line, Fig. S13b), followed by the transition from grassland to

498   forestland (red dashed line). Afforestation plays a key role in the ARF changes in East and

499   Southeast Asia, including grassland to forest, shrub to forest, and cropland to forest. These

500   three LU transitions account for 68.6% of total EA in this region. Previous reports have

501   indicated that the forest area in Southeast Asia has been decreasing in recent decades (Hansen

502   et al., 2013; Achard et al., 2002; Estoque et al., 2019) and has suffered from a net loss of 1.6

503   million ha yr^{-1} (0.6% yr^{-1}), thus, reducing the region's forest cover from 268 million ha in

504   1990 to 236 million ha in 2010 (Stibig et al., 2014). However, China has expanded the world's

505   largest afforested area since the late 1980s and had the world's largest artificial forest area in

506   2008, comprising approximately 62 million hectares (National Forest Resource Inventory

507   Report, 2009; http://www.fao.org/forestry/fra/fra2010/en/, 2010; Zhang et al., 2015).

508   Consequently, the forest cover in East and Southeast Asia has expanded accordingly. Given

509   the low albedo of forested land (Igusky et al., 2008) and the forest land expansion over the past

510   four decades (Zhang et al., 2016; Peng et al., 2014), we observed a decreasing albedo and more

511   positive ARF in these regions. In Latin America, the correlation between ARF and EA is 0.846

512   (P-value < 0.01). As shown in Fig. S13d, the annual variation of the EA nearly overlaps with

513   the transition zone between grassland and forest land. This LU transition contributes 77.4% to

514   the EA in Latin America, thereby playing a significant role in the ARF in this continent. In

515   recent decades, forest areas in Latin America have experienced a dramatic decline (Global

Forest Resources Assessment, 2020), partly due to forest wildfires (ARAGÃO et al., 2010; Escobar et al., 2019) and the transition from forest lands to pastureland under the significantly rising global demand for agricultural products (such as meat and soybeans) in this region. Correspondingly, remarkable deforestation (Armenteras et al., 2019; Bullock et al., 2020) and conversion of forest to grassland have been observed (Andela et al., 2017). Spanning almost 15 years (1990 to 2005), Latin America has been reported to have lost 7% of its forests (Da Ponte et al., 2015). This transition resulted in an increase in albedo and a decrease in ARF in Latin America (Fig. 3d).

The correlation coefficient between the ARF and the EA in Sub-Saharan Africa is 0.834 (P-value < 0.01). The EA in this region consists of the cumulative area of five net LU conversions (Table S4S6). The conversion between forestland and shrubs made the largest contribution (48.9%) to the total EA. Sub-Saharan Africa is home to most of the world's tropical grassy ecosystems (grasslands and savannas), comprising ~33.5% of Africa's landmass (Parr et al., 2014). In recent years, the forest area in Sub-Saharan Africa has decreased (Carherine et al., 2013), accompanied by an increase in savanna (including shrubs) (Atsri et al., 2018; Gaillard et al., 2018). As depicted in Fig. 3i and Fig. S13i, declining forestland in Sub-Saharan Africa consistently produces negative ARF, despite annual fluctuations.

In South Asia, the correlation coefficient between ARF and EA is 0.97 (P-value < 0.01), with the EA including the cumulative area of six net LU conversions (Table S4S6). Of these LU conversions, cropland-related LU transitions contributed up to 81.4% to the total EA. This region of Asia has experienced the most successful Green Revolution since the late 1960s (Liu et al., 2021), and India is one of the largest producers of agricultural commodities (FAOSTAT: Food and agricultural data, 2017; Teluguntla et al., 2015), with more than half of its territory used for cropland. Since the 1980s, the continuous expansion of cropland in South Asia (Hinz et al., 2020) has led to a decrease in albedo, increasing ARF (Fig. 3j and Fig. S13j). Further discussions on EA in Europe, the Near East and North Africa, North America, Oceania, and Russia, as shown in Fig. S13, are presented in Supplementary Text 6.

3.4 Response of Global ARF Change to Regional LUC Area and LU Conversion
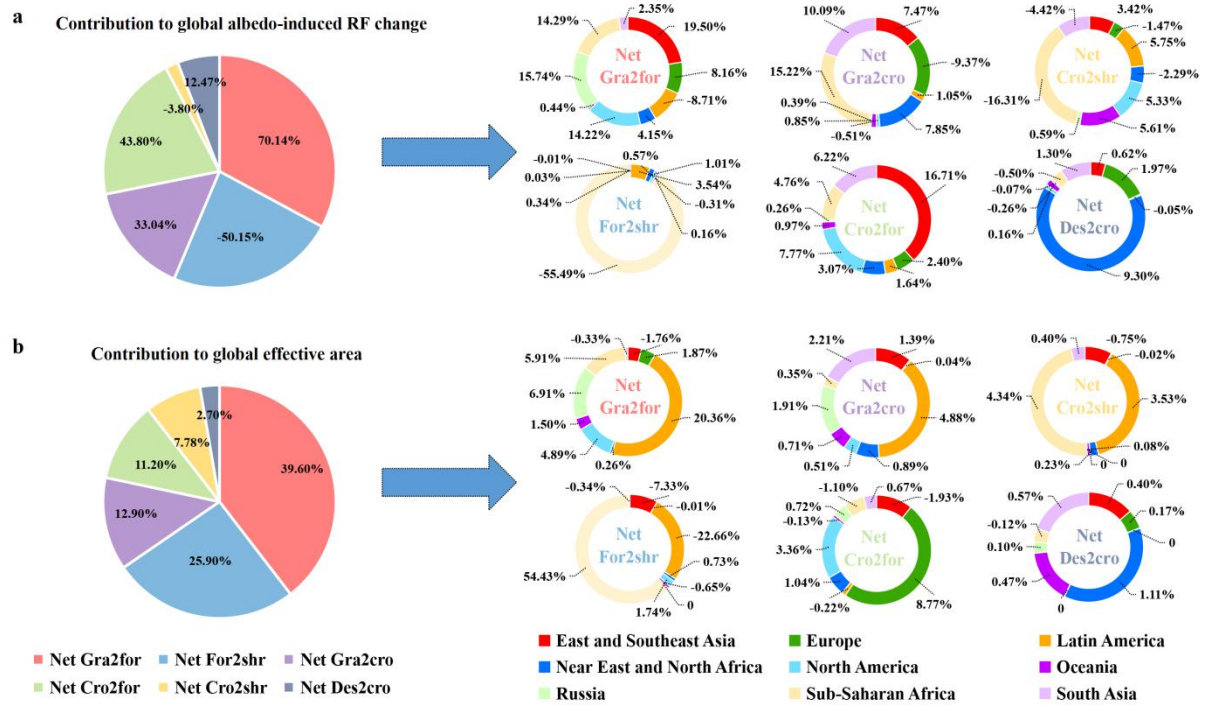
Figure 4. Contribution of six net LU conversion types in nine regions (|DC| > 1%) to the change in global ARF and EA globally and nine regions. (a) Pie charts on the left panel show the contribution of six LU conversion types in nine regions to the change in global ARF, including grassland to the forest (orange), forest to shrubs (light blue), grassland to cropland (light purple), cropland to the forest (light green), cropland to shrubs (light yellow), and desert to cropland (light gray). Donut charts on the right panel show the contribution of each of the six net LU conversion types in each of the nine regions to the change in global ARF. Among the nine regions, East and Southeast Asia are colored red, Europe deep green, Latin America deep yellow, Near East and North Africa deep blue, North America blue, Oceania purple, Russia green, Sub-Saharan Africa yellow, and South Asia purple gray. The coefficient of variation (CV) is ±5%. (b) Contribution of six LU conversions (|DC| > 1%) in the nine regions to global EA.

To quantify the contribution of each LU transition in each region to the changes in global ARF and EA, we estimated ARF and EA changes without LU conversion from 1983 to 2010 by reducing LU transition areas from 20% to 100% in 20 sensitivity experiments (see Methods), indicating no LU transition. Subsequently, we calculated the differences between ARF and EA changes with and without LU conversion to determine the contributions of any LU conversion in any region to the changes in global ARF and EA, as defined by C_{ARF} and C_{EA}, as described

563 in Eqs.5–9 of Methods. The net conversion of grasslands to forests contributed 70.14% to the

564 change in the global ARF from 1983 to 2010. During this period, the global ARF increased by

565 0.036 W m^{-2}, in line with the general upward trend. Since the albedo of grasslands is greater

566 than that of forests, we would anticipate a decrease in albedo during the transition from

567 grasslands to forests, which tends to increase the ARF. Efforts have been made to increase the

568 global forest cover through afforestation programs. However, most afforestation programs

569 have been implemented at the expense of natural vegetation, particularly grasslands, rather than

570 agricultural land (Berangere et al., 2018; Zablon et al., 2018). Globally expansive grasslands

571 were found to be suitable for future forest restoration programs to offset anthropogenic CO_2

572 emissions (Bond et al., 2016). With the updated LUC inventory with the satellite measured

573 information on a fine temporal-spatial scale, we could assess the effect of increasing forest

574 coverage on ARF with greater precision. The donut charts on the right side of Fig. 4a depict

575 the change in global ARF due to LU conversions in each of the nine regions. The results

576 indicate that grassland to forest conversion in East and Southeast Asia contributes 19.50% to

577 the change in global ARF, 8.16% from Europe, −8.71% from Latin America, 4.15% from the

578 Near East and North Africa, 14.22% from North America, 0.44% from Oceania, 15.74% from

579 Russia, 14.29% from Sub-Saharan Africa, and 2.35% from South Asia, respectively. The

580 global net conversion of forests to shrubs contributes −50.15% to the change in global ARF,

581 with individual contributions from East and Southeast Asia (0.16%), Europe (−0.01%), Latin

582 America (3.54%), Near East and North Africa (1.01%), North America (0.57%), Oceania

583 (−0.31%), Russia (0.03%), Sub-Saharan Africa (−55.49%), and South Asia (0.35%). Thus, the

584 contribution of the net conversion of forests to shrubs to the global ARF change enhanced the

585 cooling effect. The contributions from the remaining four net conversion types are shown in

586 Table ~~S6~~S8.

587   The contributions of net conversion from grassland to forest, forest to shrubs, grassland

588 to cropland, cropland to the forest, cropland to shrubs, and desert to cropland to the global EA

589 (Eq. (4)) are 39.60%, 25.90%, 12.90%, 11.20%, 7.78%, and 2.70%, respectively, as depicted

590 in the pie charts on the left panel of Fig. 4b. The contributions of the six net conversion types

591 in each of nine regions to the global EA are displayed in donut charts in the right panel of Fig.

592 4b, providing additional information regarding the impact of regional LU conversion on the

593 variation in global ARF. For instance, the contributions of net conversion type of grassland to

594 forest in each of the nine regions to the global EA are as follows: −1.76% from East and

595 Southeast Asia, 1.87% from Europe, 20.36% from Latin America, 0.26% from Near East and

596 North Africa, 4.89% from North America, 1.49% from Oceania, 6.91% from Russia, 5.91%

597 from Sub-Saharan Africa, and −0.33% from South Asia. Additional results for the remaining

598 five types of net conversion in each of the nine regions are presented in Table S7S9.

3.5 Contributions of Two-way LU Conversion to Global ARF Change

600
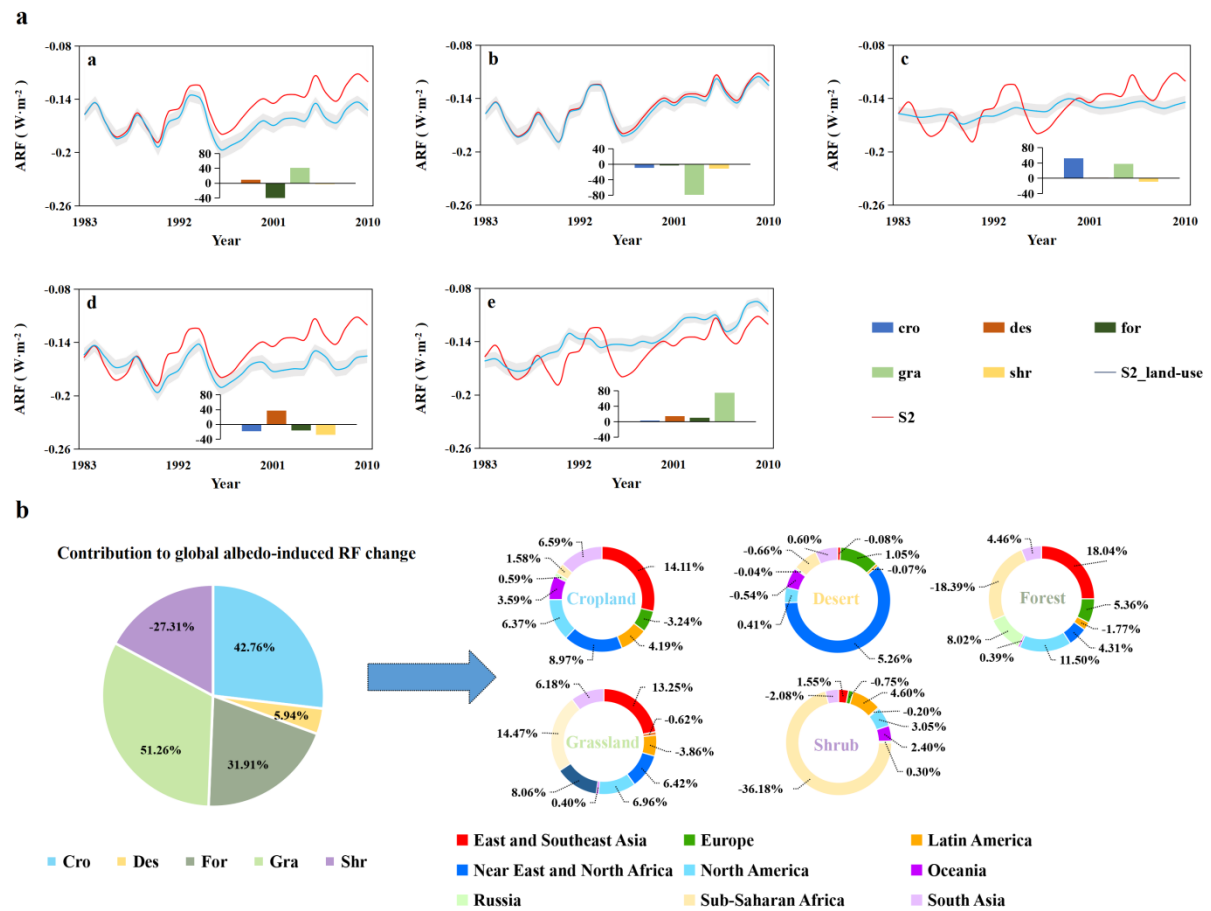
601 **Figure 5.** Changes in global ARF derived from model scenario 2 (S2) and contribution of five LU types in

602 the globe and nine regions to the change in global ARF. (a) Changes in global ARF subject to LU transition

603 from 1983 to 2010 (solid red line) and a fixed LU type without transition (solid blue line) for five LU types,

including croplands (cro, Fig. 5a-a), deserts (des, Fig. 5a-b), forests (for, Fig. 5a-c), grasslands (gra, Fig. 5a-d), and shrublands (shr, Fig. 5a-e). The inset bar chart represents the relative contribution of the two-way LU net transition between the LU of the interested and other LUs from 1983 to 2010. Taking the bar chart in Fig. 5a-a as an example, the bars with different colors show the result of the two-way transition between cropland and other LU types from 1983 to 2010. Positive bars represent the conversion from other LU types to cropland, and negative bars indicate the transition from cropland to other LU types. Shadings in Fig. 5a-a–5a-e indicate the uncertainty interval estimated by Monte Carlo simulations. (b) Contribution of five LU types in each region to changes in global ARF. The pie chart on the left panel shows the contribution of five LU types to the change in ARF in the globe, including cropland (light blue), desert (light yellow), forest (gray-green), grassland (light green), and shrubs (light purple). Five small donut charts on the right panel show the contribution of each type in each of the nine regions to changes in global ARF. The coefficient of variation (CV) is ±5%.

We also set up 20 sensitivity experiments to examine the response of ARF to two-way LU transition in each region. The two-way LU transition entails LU conversion from a particular LU type to the remaining 4 LU types and vice versa, which accounts for eight LU conversions for the five LU types in the GLASS-GLS inventory. We compare the changes in global ARF driven by LU transition from 1983 to 2010 to the ARF estimated by reducing LU transition areas from 20% to 100%. The 100% reduction of LU transition area means no LU transition. As an illustration, Fig. 5a-a compares the change in global ARF caused by the transition between cropland and the other four LUs (cropland to desert, forest, grass, and shrub, solid red line) and without transition (fixed cropland, solid blue line). Marked differences can be observed for both with and without the transition between croplands and other LU types. The trend and annual fluctuation of ARF are consistent with the results subject to LU transition (solid red line). However, under the fixed cropland (no LU transition) during this period (solid blue line), the negative values of ARF change have decreased since 1990 in comparison to the case with LU transition. As shown in the inset of Fig. 5a-a, the transition from grassland to cropland accounts for 41.0% of the cropland transition area, while the net transition from desert to cropland accounts for 9.2%. The remaining two net LU transitions occurred from croplands to forests (−48.9%) and shrubs (−0.9%), respectively, implying that LU transitions from croplands to other LUs account for −49.8% of the cropland transition area. By combining these

transition areas, the net cropland transition area was calculated to be 0.4%, indicating the growth of cropland (Fig. S1). Since the transition from grasslands to croplands decreased surface albedo (Table S2S3), the LU conversion in this instance decreases the absolute value of negative ARF, thereby weakening the cooling effect.

Using the GLASS-GLC inventory (scenario 2), we further estimated the percentage change (%) in global ARF with the transition between cropland and the other four LUs (solid red line, Fig. S14a) from 1983 to 2010. During this period, the percentage changes ranged from −0.6% to 28.4%, illustrating a significant upward trend. From 1998 to 2010, the annual percentage change in global ARF was almost 15%, indicating that the cropland transition significantly contributed to the change in global ARF. We also observed an overall increase in cropland area from 1983 to 2010, as indicated by the positive accumulated cropland area in Fig. S14a (solid black line, scaled to the right of the Y-axis), which is consistent with the growth rate of cropland area of 0.037 Mha/yr during this period.

Similarly, Fig. 5a-b–5a-e illustrate OSCAR-modeled global ARF variation utilizing GLASS-GLC inventory with and without LU transition of individual LU types from 1983 to 2010. As shown in Fig. 5a-b, the conversion of the desert to other LU types has little effect on the global ARF variation, and the modeled ARF from simulations with and without LU transition is nearly identical. Fig. S14b demonstrates that the percentage change in the global ARF was less than 4.2% between 1983 and 2010, with a mean value of 1.7%. As illustrated in the inset of Fig. 5a-b, the net transition from desert to grassland (light green bar) accounts for 79.1% of the total transition area, the net transition from desert to shrubs (light yellow bar) accounts for 11.5% of the total transition area, and the net transition from desert to cropland (deep blue bar) accounts for 8.9% of the total transition area, respectively. The percentage change indicates a net decrease in a desert land, which is supported by the declining accumulated area of desert land (Fig. S14b). The lack of significant differences between global ARF with and without LU transition is most likely due to the smaller change in the desert area over the past decades. Detailed discussions of the variations in ARF induced by forest, grassland, and shrub transitions utilizing the GLASS-GLC inventory, as depicted in Fig. 5a-c–5a-e are presented in Supplementary Text 7. Overall, Fig. 5a reveals an increasing trend of

ARF change, highlighted by attenuated negative ARF from 1983 to 2010, which suggests a weakening cooling effect by the global ARF (Fig. 1).

Fig. 5b depicts the contribution of regional LU transactions to the change in global ARF (five pie charts on the right panel of Fig. 5b). Cropland, desert, forest, grassland, and shrubs contributed 42.76%, 5.94%, 31.91%, 51.26%, and −27.31%, respectively, to the change in global ARF, as depicted in the pie chart on the left panel of in Fig. 5b. The donut charts on the right panel of Fig. 5b illustrate the contribution of each of the five LU types in the nine regions to the change in the global ARF. Taking cropland as an example, the contributions of cropland-related conversions in each of the nine regions to the change in global ARF are as follows: 14.11% (East and Southeast Asia), −3.24% (Europe), 4.19% (Latin America), 8.97% (Near East and North Africa), 6.37% (North America), 3.59% (Oceania), 0.59% (Russia), 1.58% (Sub-Saharan Africa), and 6.59% (South Asia). As stated previously and depicted in the left panel of Fig. 5b, the sum of the contributions from these nine regions to the global ARF change is 42.76%. As a result, cropland-related LU conversion in East and Southeast Asia (primarily China) made the largest contribution to global ARF variation. The results for the remaining four LU types are presented in Table ~~S8~~S5.

4. Discussion

By incorporating a recently developed satellite-remote sensing-based high-resolution LUC dataset into the OSCAR model, we demonstrate that previous estimates of ARF derived from historical statistics-based LUH1-LUC data with a coarse resolution tend to overestimate the LUC driving albedo-induced cooling effect. Our revised estimate reveals that the global ARF (-0.12 W m^{-2}) is lower than the value adopted by the IPCC (-0.15 W m^{-2}). Our results indicate that, among the nine selected regions covering the global land area, Sub-Saharan Africa made the largest net contribution (39.2%) to the global mean ARF (-0.06 W m^{-2}) owing to the transition of forestland to shrubland, which result in greater surface albedo and, hence, declining ARF. The latter became very significant from 1982 to 2010. East and Southeast Asia also contributed significantly, following Sub-Saharan Africa, to the changes in global ARF at

692 33.6% (0.016 W m^{-2}) due to the LU conversion from the grassland to forest conversion and

693 land desertification management, which result in lower surface albedo (Table ~~S2~~S3) and

694 increasing ARF. In line with previous researches, we demonstrate that RF induced by changes

695 in surface albedo is primarily driven by changes in vegetation (Betts et al., 2000). The

696 transformation from forest to grass, shrub, and crop, and crop to grass resulted in decrease in

697 ARF of −0.68 W m^{-2}, −0.48 W m^{-2}, −0.19 W m^{-2}, and −0.22 W m^{-2}, respectively, due to the

698 enhancement of surface albedo by the transformation from forest to these vegetation types.

699 Opposite conversions of these vegetation types to forests outweigh positive contributions to

700 ARF, indicating a rise in surface albedos and cooling effects. In addition to the magnitudes, we

701 find that the two LUC datasets developed based on different data sources, approaches, and

702 resolutions produce different ARFs, indicating that LUC data influenced considerably on

703 regional and continental ARFs.

704   Notably, the present study only predicts ARF and its change induced by surface albedo

705 subject to LUC and LU conversions but does not address RF driven by CO_2 emissions as a

706 result of carbon source-sink conversions associated with LUC and the ARF associated with the

707 LULCC-induced changes in snow cover. However, the major findings of dominant LU

708 transition patterns between forest and grassland/shrub/cropland imply CO_2 source-sink

709 transitions, which are expected to influence LUC-driven RF more strongly. On the one hand,

710 the unexpectedly weaker cooling effect of LUC observed in this study indicates that global LU

711 and LU conversion as carbon sinks since the 1980s do not significantly mitigate climate

712 warming. On the other hand, land management must be improved by increasing the capacity

713 of LUC for carbon sequestration, preserving carbon sinks, and providing renewable resources.

714 Our results show that Sub-Saharan Africa contributed the most to the forest-to-grass and forest-

715 to-shrub transition-induced global ARF, with predicted ARF values of −0.20 W m^{-2} and −0.40

716 W m^{-2}, respectively. In addition, East and Southeast Asia contribute the most to the ARF due

717 to the conversion of LU from forest to crop and crop to grass. Furthermore, Sub-Saharan Africa

718 has also been confirmed to have the highest proportion of forest-to-grass and forest-to-shrub

719 transitions, contributing to a cooling effect.

720   These findings have substantial ramifications for pertinent policy issues. Accordingly,
721 they suggest that local governments and international communities should take more action in
722 Sub-Saharan Africa to slow down or, preferably, stop deforestation and forest-to-grassland-
723 and-cropland conversion, which is a significant contributor to carbon emission enhancement
724 (Spawn et al., 2019; Pendrill et al., 2019; Chang et al., 2021). In our case, even though this LU
725 transition increases surface albedo, thereby increasing LUC-albedo–induced negative RF and
726 exerting a cooling effect, this effect is negligible compared to the increase in RF caused by
727 CO_2 emissions (IPCC AR6, 2021; Li et al., 2016; Jian et al., 2022). Therefore, the cooling
728 effect of afforestation on reducing CO_2 emissions outweighs the warming effect of the resultant
729 decrease in surface albedo. The crop-to-forest transition occurring primarily in East and
730 Southeast Asia, Europe, and the Near East and North Africa has been partially encouraged by
731 national and international cropland and water resource conservation strategies and programs,
732 resulting in ARF values of 0.09 W m^{-2}, 0.02 W m^{-2}, and 0.01 W m^{-2}, respectively. The "Grain-
733 for-Green" program in northwestern China (Wang et al., 2023), for example, impedes the
734 transition from crop to forest in East and Southeast Asia. Although the program helps improve
735 the ecological environment, from the perspective of ARF, it tends to reduce the surface albedo
736 and increase positive RF, thereby enhancing the warming effect. It is worth noting that the
737 present study did not incorporate non-radiative process and the coupling between land and
738 atmosphere, which might drive many feedback mechanisms. The significance of land
739 management in maintaining carbon sinks and providing renewable resources was also not dealt
740 with. However, this study provides additional evidence of the importance of land management
741 in influencing the carbon sinks. Optimal land management should implement integrated and
742 enforceable sustainable agriculture, climate-smart forestry, and climate-friendly land resources
743 with co-benefits and cost-efficiency.
744

745 **5. Conclusions**
746   We have improved the global and the nine regional ARF simulations using OSCAR model
747 a updated LUC dataset on a high temporal-spatial resolution. We explored the causes of ARF
748 changes in the world and nine regions across the globe by disentangling land change data for

749   20 transformation types. We also developed the concepts of DC and EA to better explain the

750   changes in ARFs. The major findings are summarized below:

751   • The magnitude of the negative ARF obtained from this study is 20% lower than previous

752   estimations, implying a weaker cooling effect. The results suggest that global LUC-

753   induced changes in surface albedo may not significantly slow global warming as

754   previously expected.

755   • Sub-Saharan Africa made the largest net contribution to the global ARF (39.2%) due to

756   significant land-use conversions, typically from forest to other vegetation land

757   accompanying with higher surface albedo. The most significant land cover changes

758   occurred in East and Southeast Asia, which dominated (33.6%) the changes in global ARF

759   in recent decades.

760   • The largest change in global ARF occurs in the net transition from grassland to forest,

761   contributing 70.14% to LUC-induced ARF. Of which, East and Southeast Asia region

762   accounts for 19.50% of the change in global ARF. The net transition from forest to shrub

763   made the largest negative contribution of -50.15% to the LUC-induced change in global

764   ARF, of which Sub-Saharan Africa accounted for -55.49% to the change in global ARF.

765   • Vegetation lands exert a most vital effect on global ARF variation, of which grassland

766   contributed 51.26%. Among those vegetation lands, the changes in grasslands in Sub-

767   Saharan Africa contributed 14.47% to the global ARF variation subject to the vegetation

768   land transition, followed by East and Southeast Asia at 13.25%.

769

770

771

772   **Code availability**

773   OSCAR v2.4 source code is available for downloading on https://github.com/tgasser/OSCAR.

774

775   **Data availability**

776   GLASS-GLC data can be accessed at https://doi.org/10.1594/PANGAEA.913496. The dataset
777   used to generate all the results of this study is available at
778   https://doi.org/10.5281/zenodo.14586249.

779

Author contributions

All authors contributed to the manuscript and have given approval of the final version. XZ coordinated and supervised the project. XZ, XJ and JM designed the present experiment, carried out modeling, and drafted the manuscript. HG, YZ and RZ collected the data. XL, KC, TH, ST and JL analyzed simulation results.

Competing interests

The authors declare that they have no known competing financial interests or personal relationships that could have appeared to influence the work reported in this paper.

Acknowledgements

We wish to thank the High-performance Computing Platform of Peking University to support extensive model simulations of this study. We acknowledge the use of OSCAR model and GLASS-GLC dataset.

Financial support

This study is supported by National Key R&D Program of China (2023YFE0112900) and the National Natural Science Foundation of China (42407134, 41991312, and 41977357).

References

Achard, F., Eva, H. D., Stibig, H. J., Mayaux, P., Gallego, J., Richards, T., and Malingreau, J. P.: Determination of Deforestation Rates of the World's Humid Tropical Forests, Science, 297, 999–1002, https://doi.org/10.1126/science.1070656, 2002.

Andela, N., Morton, D. C., Chen, L. G. Y., Werf, G. R. V. D., Kasibhatla, P. S., Defries, R. S., Collatz, G. J., Hantson, S., Kloster, S., Bachelet, D., Forrest, M., Lasslop, G., Li, F., Mangeon, S., Melton, J. R., Yue, C., and Randerson, J. T.: A human-driven decline in global burned area, Science, 356, 1356–1362, https://doi.org/10.1126/science.aal4108, 2017.

Andrade, B. O., Koch, C., Boldrini, I. I., Martin, E. V., Hasenack, H., Hermann, J. M., Kollmann, J., Pillar, V. D., and Overbeck, G. E.: Grassland degradation and restoration: a conceptual framework of stages and thresholds illustrated by southern Brazilian grasslands, Nat. & Conserv., 13, 95–104, https://doi.org/10.1016/J.NCON.2015.08.002, 2015.

Andrews, D.: An Introduction to Atmospheric Physics (2nd edition), Cambridge University Press, ISBN, 9780511800788, https://doi.org/10.1017/CBO9780511800788, 2012.

Andrews, T., Betts, R. A., Booth, B. B. B., Jones, C. D., and Jones, G. S.: Effective radiative forcing from historical land use change, Clim. Dyn., 48, 3489–3505, https://doi.org/10.1007/s00382-016-3280-7, 2017.

Andrews, T., and Forster, P. M.: Energy budget constraints on historical radiative forcing, Nat. Clim. Chang., 10, 313–316, https://doi.org/10.1038/s41558-020-0696-1, 2020.

ARAGÃO, L. E. O. C., and Shimabukuro, Y. E.: The Incidence of Fire in Amazonian Forests with Implications for REDD, Science, 328, 1275–1278, httos://doi.org/10.1126/science.1186925, 2010.

Armenteras, D., Schneider, L., and Dávalos, L. M.: Fires in protected areas reveal unforeseen costs of Colombian peace, Nat. Ecol. Evol., 3, 20–23, https://doi.org/10.1038/s41559-018-0727-8, 2019.

Armenteras, D., Dávalos, L. M., Barreto, J. S., Miranda, A., Hernández-moreno, A., Zamorano-elgueta, C., González-delgado, T. M., Meza-elizalde, M. C., and Retana, J.: Fire-induced loss of the world's most biodiverse forests in Latin America, Sci. Adv., 7, eabd3357, https://doi.org/10.1126/sciadv.abd3357, 2021.

Atsri, H. K., Konko, Y., Cuni-Sanchez, A., Abotsi, K. E., and Kokou, K.: Changes in the West African forest-savanna mosaic, insights from central Togo, Plos One, 13, e0203999, https://doi.org/10.1371/journal.pone.0203999, 2018.

Aune, S., Bryn, A., and Hovstad, K. A.: Loss of semi-natural grassland in a boreal landscape: impacts of agricultural intensification and abandonment, J. Land Use Sci., 13, 375–390, https://doi.org/10.1080/1747423X.2018.1539779, 2018.

Bardgett, R. D., Bullock, J. M., Lavorel, S., Manning, P., Schaffner, U., Ostle, N., Chomel, M., Durigan, G., Fry, E. L., Johnson, D., Lavallee, J. M., Provost, G. L., Luo, S., Png, K., Sankaran, M., Hou, X. Y., Zhou, H. K., Ma, L., Ren, W. B., Li, X. L., Ding, Y., Li, Y. H., and Shi, H. X.: Combatting global grassland degradation, Nat. Rev. Earth Environ., 2, 720–735, https://doi.org/10.1038/s43017-021-00207-2, 2021.

Berangere, A. L., Jennifer, R. M., Charles, U., and Boris, V.: Global fire history of grassland biomes, Ecol. Evol., 8, 8831–8852, https://doi.org/10.1002/ece3.4394, 2018.

Betts, R. A.: Offset of the potential carbon sink from boreal forestation by decreases in surface albedo, Nature, 408, 187–190, https://doi.org/10.1038/35041545, 2000.

Betts, R. A., Falloon, P. D., Goldewijk, K. K., and Ramankutty, N.: Biogeophysical effects of land use on climate: Model simulations of radiative forcing and large-scale temperature change, Agric. For. Meteorol., 142, 216–233,

https://doi.org/10.1016/j.agrformet.2006.08.021, 2007.

Bonan, G. B.: Forests and Climate Change: Forcings, Feedbacks, and the Climate Benefits of Forests, Science, 320, 1444–1449, https://doi.org/10.1126/science.1155121, 2008.

Bond, W. J.: Ancient grasslands at risk, Science, 351, 120–122, https://doi.org/10.1126/science.aad5132, 2016.

Bullock, E. L., Woodcock, C. E., Jr, C. S., and Olofsson, P.: Satellite-based estimates reveal widespread forest degradation in the Amazon, Glob. Chang. Biol., 26, 2956–2969, https://doi.org/10.1111/gcb.15029, 2020.

Cai, M., and Kalnay, E.: Impact of land-use change on climate, Nature, 427, 214, https://doi.org/10.1038/427214a, 2004.

Catherine, B., Andreas, B. B., Francois, D., Andrea, L., Philippe, M., and Frédéric, A.: Continental estimates of forest cover and forest cover changes in the dry ecosystems of Africa between 1990 and 2000, J. Biogeogr., 40, 1036–1047, https://doi.org/10.1111/jbi.12084, 2013.

Chang, J., Philippe, C., Thomas, G., Pete, S., Mario, H., Petr, H., Michael, O., Bertrand G., Daniel, S. G., Li, W., Victoria, N., Peng, S. S., Qiu, C. J., Tian, H. Q., Nicolas, V., Yue, C., and Zhu, D.: Climate warming from managed grasslands cancels the cooling effect of carbon sinks in sparsely grazed and natural grasslands, Nat. Commun., 12, 118, https://doi.org/10.1038/s41467-020-20406-7, 2021.

Da, P. E., Fleckenstein, M., Leinenkugel, P., Parker, A., Oppelt, N., and Kuenzer, C.: Tropical forest cover dynamics for Latin America using Earth observation data: a review covering the continental, regional, and local scale, Int. J. Remote Sens., 36, 3196–3342, https://doi.org/10.1080/01431161.2015.1058539, 2015.

Davidson, E. A., Alessandro, C. D. A., Paulo, A., Jennifer, K., Balch., Brown, F. I., Mercedes, M. C. B., Michael, T. C., Ruth, S., Defries., Michael, K., Marcos, L., Munger, J. W., Schroeder, W., Britaldo, S. S. F., Carlos, M. S., and Steven, C. W.: The Amazon basin in transition, Nature, 481, 321–328, https://doi.org/10.1038/nature10717, 2012.

Edouard, L. D., and Nathalie, D. N. D.: Climatic Impact of Global-Scale Deforestation: Radiative versus Nonradiative Processes, J. Climate, 23, 97–112, https://doi.org/10.1175/2009JCLI3102.1, 2010.

Escobar, H.: Bolsonaro's first moves have Brazilian scientists worried, Science, 363, 330, https://doi.org/10.1126/science.363.6425.330, 2019.

Estoque, R. C., Ooba, M., Avitabile, V., Hijioka, Y., DasGupta, R., Togawa, T., and Murayama, Y.: The future of Southeast Asia's forests, Nat. Commun., 10, 1829, https://doi.org/10.1038/s41467-019-09646-4, 2019.

FAO, FAOSTAT: Food and agricultural data, Retrieved September 25, 2017.

Feddema, J. J., Oleson, K. W., Bonan, G. B., Mearns, L. O., Buja, L. E., Meehl, G. A., and Washington, W. M.: The Importance of Land-Cover Change in Simulating Future Climates, Science, 310, 1674–1678, https://doi.org/10.1126/science.1118160, 2005.

Foley, J. A., Defries, R., Asner, G. P., Barford, C., Bonan, G., Carpenter, S. R., Chapin, F. S., Coe, M. T., Daily, G. C., Gibbs, H. K., Helkowski, J. H., Holloway, T., Howard, E. A., Kucharik, C. J., Monfreda, C., Patz, J. A., Prentice, I. C., Ramankutty, N., and Snyder, P. K.: Global Consequences of Land Use, Science, 309, 570–574, https://doi.org/10.1126/science.1111772, 2005.

Food and Agriculture Organization of the United Nations (FAO), Global Forest Resources Assessment 2010, Available at: http://www.fao.org/forestry/fra/fra2010/en, 2010.

Food and Agriculture Organization of the United Nations, Global Forest Resources Assessment 2020.

Forster, P., Ramaswamy, V., Artaxo, P., Berntsen, T., Betts, R., Fahey, D. W., Haywood, J., Lean, J., Lowe, D. C., Myhre, G., Nganga, J., Prinn, R., Raga, G., Schulz, M., and Dorland, R. V.: Changes in Atmospheric Constituents and in Radiative Forcing. In: Climate Change 2007: The Physical Science Basis. Contribution of Working Group I to the Fourth Assessment Report of the Intergovernmental Panel on Climate Change [Solomon, S., Qin, D., Manning, M., Chen, Z., Marquis, M., Averyt, K. B., Tignor, M., and Miller, H. L. Cambridge University Press, Cambridge, United Kingdom and New York, NY, USA, 2007.

Gaillard, C., Langan, L., Pfeiffer, M., Kumar, D., Martens, C., Higgins, S. I., and Scheiter, S.: African shrub distribution emerges via a trade-off between height and sapwood conductivity, J. Biogeogr., 45, 2815–2826, https://doi.org/10.1111/jbi.13447, 2018.

Gasser, T., Ciais, P., Boucher, O., Quilcaille, Y., Tortora, M., Bopp, L., and Hauglustaine, D.: The compact Earth system model OSCAR v2.2: description and first results, Geosci. Model Dev., 10, 271–319, https://doi.org/10.5194/gmd-10-271-2017, 2017.

Gong, P., Wang, J., Yu, L., Zhao, Y. C., Zhao, Y. Y., Liang, L., Niu, Z., Huang, X. M., Fu, H. H., Liu, S., Li, C. C., Li, X. Y., Fu, W., Liu, C. X., Xu, Y., Wang, X. Y., Cheng, Q., Hu, L. Y., Yao, W. B., Zhang, H., Zhu, P., Zhao, Z. Y., Zhang, H. Y., Zheng, Y. M., Ji, L. Y., Zhang, Y. W., Chen, H., Yan, A., Guo, J. H., Yu, L., Wang, L., Liu, X. J., Shi, T. T., Zhu, M. H., Chen, Y. L., Yang, G. W., Tang, P., Xu, B., Giri, C., Clinton, N., Zhu, Z. L., Chen,

J., and Chen, J.: Finer resolution observation and monitoring of global land cover: first mapping results with Landsat TM and ETM+ data, Int. J. Remote Sens., 34, 2607–2654, https://doi.org/10.1080/01431161.2012.748992, 2013.

Gries, T., Redlin, M., and Ugarte, J. E.: Human-induced climate change: the impact of land-use change, Theor. Appl. Climatol., 135, 1031–1044, https://doi.org/10.1007/s00704-018-2422-8, ~~2018~~2019.

Hansen, J., and Nazarenko, L.: Soot climate forcing via snow and ice albedos, Proc. Natl. Acad. Sci. U.S.A., 101, 423–428, https://doi.org/10.1073/pnas.2237157100, 2003.

Hansen, M. C., Potapov, P. V., Moore, R., Hancher, M., Turubanova, S. A., Tyukavina, A., Thau, D., Stehman, S. V., Goetz, S. J., Loveland, T. R., Kommareddy, A., Egorov, A., Chini, L., Justice, C. O., and Townshend, J. R. G.: High-Resolution Global Maps of 21st-Century Forest Cover Change, Science, 342, 850–853, https://doi.org/10.1126/science.1244693, 2013.

Hinz, R., Sulser, T. B., Huefner, R., Croz, D. M. D., Dunston, S., Nautiyal, S., Ringler, C., Schuengel, J., Tikhile, P., Wimmer, F., and Schaldach, R.: Agricultural Development and Land Use Change in India: A Scenario Analysis of Trade-Offs Between UN Sustainable Development Goals (SDGs), Earth's Future, 8, e2019EF001287, https://doi.org/10.1029/2019EF001287, 2020.

Houghton, R. A., House, J. I., Pongratz, J., Werf, G. R. V. D., Defries, R. S., Hansen, M. C., Quéré, C. L., and Ramankutty, N.: Carbon emissions from land use and land-cover change, Biogeosciences, 9, 5125–5142, https://doi.org/10.5194/bg-9-5125-2012, 2012.

Huang, T., Ma, J. M., Song, S. J., Ling, Z. L., Macdonald, R. W., Gao, H., Tao, S., Shen, H. Z., Zhao, Y., Liu, X. R., Tian, C. G., Li, Y. F., Jia, H. L., Lian, L. L., and Mao, X. X.: Health and environmental consequences of crop residue burning correlated with increasing crop yields midst India's Green Revolution, Npj. Clim. Atmos. Sci., 5, 81, https://doi.org/10.1038/s41612-022-00306-x, 2022.

Hurtt, G. C., Chini, L. P., Frolking, S., Betts, R. A., Feddema, J., Fischer, G., Fisk, J. P., Hibbard, K., Houghton, R. A., Janetos, A., Jones, C. D., Kindermann, G., Kinoshita, T., Goldwijk, K. K., Riahi, K., Shevliakova, E., Smith, S., Stehfest, E., Thomson, A., Thornton, P., Vuuren, D. P. V., and Wang, Y. P.: Harmonization of land-use scenarios for the period 1500-2100: 600 years of global gridded annual land-use transitions, wood harvest, and resulting secondary lands, Clim. Chang., 109, 117–161, https://doi.org/10.1007/s10584-011-0153-2, 2011.

Hurtt, G. C., Chini, L., Sahajpal, R., Frolking, S., Bodirsky, B. L., Calvin, K., Doelman, J. C., Fisk, J., Fujimori, S., Goldewijk, K. K., Hasegawa, T., Havlik, P., Heinimann, A.,

Humpenöder, F., Jungclaus, J., Kaplan, J. O., Kennedy, J., Krisztin, T., Lawrence, D., Lawrence, P., Ma, L., Mertz, O., Pongratz, J., Popp, A., Poulter, B., Riahi, K., Shevliakova, E., Stehfest, E., Thornton, P., Tubiello, F. N., Vuuren, D. P. V., and Zhang, X.: Harmonization of global land use change and management for the period 850-2100 (LUH2) for CMIP6, Geosci. Model Dev., 13, 5425–5464, https://doi.org/10.5194/gmd-13-5425-2020, 2020.

Igusky, K.: Quantifying Albedo and Surface Temperature over Different Land Covers: Implications for Carbon Offsets, Duke University Press, 2008.

Imai, N., Furukawa, T., Tsujino, R., Kitamura, S., and Yumoto, T.: Factors affecting forest area change in Southeast Asia during 1980-2010, Plos One, 13, e0197391, https://doi.org/10.1371/journal.pone.0197391, 2018.

Intergovernmental Panel on Climate Change (IPCC), Climate Change 2001: The Scientific Basis is the most comprehensive and up-to-date scientific assessment of past, present and future climate change, Cambridge University Press, Cambridge, United Kingdom and New York, NY, USA, 2001.

Intergovernmental Panel on Climate Change (IPCC), Climate change 2021: The physical science basis, the working Group I contribution to the sixth assessment report of the intergovernmental panel on climate change, Cambridge University Press, Cambridge, United Kingdom and New York, NY, USA, 2021.

Jackson, R. B., Randerson, J. T., Canadell, J. G., Amderson, R. G., Avissar, R., Baldocchi, D. D., Bonan, G. B., Caldeira, K., Diffenbaugh, N. S., Field, C. B., Hungate, B. A., Jobbágy, E. G., Kueppers, L. M., Nosetto, M. D., and Pataki, D. E.: Protecting climate with forests, Environ. Res. Lett., 3, 044006, https://doi.org/10.1088/1748-9326/3/4/044006, 2008.

Jian, X. H., Zhang, X. D., Liu, Y. J., Liu, X. R., Chen, K. J., Wang, L. F., Li, J. X., Zhao, Y., Luo, J. M., Zhugu, R. Y., and Ma, J. M.: The Response of Radiative Forcing to High Spatiotemporally Resolved Land-Use Change and Transition From 1982 to 2010 in China, Geophys. Res. Lett., 49, e2022GL099003, https://doi.org/10.1029/2022GL099003, 2022.

Jiao, T., Williams, C. A., Ghimire, B., Masek, J., Gao, F., and Schaaf, C.: Global climate forcing from albedo change caused by large-scale deforestation and reforestation: quantification and attribution of geographic variation, Clim. Chang., 142, 463–476, https://doi.org/10.1007/s10584-017-1962-8, 2017.

Keenan, R. J., Reams, G. A., Achard, F., Freitas, J. V. D., Grainger, A., and Lindquist, E.: Dynamics of global forest area: Results from the FAO Global Forest Resources Assessment 2015, For. Ecol. Manag., 353, 9–20, https://doi.org/10.1016/j.foreco.2015.06.014, 2015.

Lark, T. J., Spawn, S. A., Bougie, M., and Gibbs, H. K.: Cropland expansion in the United States produces marginal yields at high costs to wildlife, Nat. Commun., 11, 4295, https://doi.org/10.1038/s41467-020-18045-z, 2020.

Li, B. G., Gasser, T., Ciais, P., Piao, S. L., Tao, S., Balkanski, Y., Hauglustaine, D., Boisier, J. P., Chen, Z., Huang, M. T., Li, L. Z. X., Li, Y., Liu, H. Y., Liu, H. F., Peng, S. S., Shen, Z. H., Sun, Z. Z., Wang, R., Wang, T., Yin, G. D., Yin, Y., Zeng, H., Zeng, Z. Z., and Zhou, F.: The contribution of China's emissions to global climate forcing, Nature, 531, 357–361, https://doi.org/10.1038/nature17165, 2016.

Liu, H., Gong, P., Wang, J., Clinton, N., Bai, Y. Q., and Liang, S. L.: Annual dynamics of global land cover and its long-term changes from 1982 to 2015, Earth Syst. Sci. Data, 12, 1217–1243, https://doi.org/10.5194/essd-12-1217-2020, 2020.

Liu, X. R., Zhang, X. D., Huang, Y. F., Chen, K, J., Wang, L. F., Ma, J. M., Huang, T., Zhao, Y., Gao, H., Tao, S., Liu, J. F., Jian, X. H., and Luo, J. M.: The Direct Radiative Forcing Impact of Agriculture-Emitted Black Carbon Associated With India's Green Revolution, Earth's Future, 9, e2021EF001975, https://doi.org/10.1029/2021EF001975, 2021.

Liu, X. Y., and Xin, L. J.: China's deserts greening and response to climate variability and human activities, Plos One, 16, e0256462, https://doi.org/10.1371/journal.pone.0256462, 2021.

Mograbi, P. J., Erasmus, B. F. N., Witkowski, E. T. F., Asner, G. P., Wessels, K. J., Mathieu, R., Knapp, D. E., Martin, R. E., and Main R.: Biomass Increases Go under Cover: Woody Vegetation Dynamics in South African Rangelands, Plos One, 10, e0127093, https://doi.org/10.1371/journal.pone.0127093, 2015.

Myhre, G., and Myhre, A.: Uncertainties in Radiative Forcing due to Surface Albedo Changes Caused by Land-Use Changes, J. Climate, 16, 1511–1524, https://doi.org/10.1175/1520-0442(2003)016<1511:UIRFDT>2.0.CO;2, 2003.

Nogueira, D. S., Marimon, B. S., Marimon-Junior, B. H., Oliveira, E. A., Morandi, P., Reis, S. M., Elias, F., Neves, E. C., Feldpausch, T. R., Lloyd, J., and Phillips, O. L.: Impacts of Fire on Forest Biomass Dynamics at the Southern Amazon Edge, Environ. Conser., 46, 285–292, https://doi.org/10.1017/S0376892919000110, 2019.

Ouyang, Z. T., Sciusco, P., Jiao, T., Feron, S., Lei, C., Li, F., John, R., Fan, P., Li, X., Williams, C. A., Chen, G. Z., Wang, C. H., and Chen, J. Q.: Albedo changes caused by future urbanization contribute to global warming, Nat. Commun., 13, 3800, https://doi.org/10.1038/s41467-022-31558-z, 2022.

Parr, C. L., Lehmann, C. E. R., Bond, W. J., Hoffmann, W. A., and Andersen, A. N.: Tropical

grassy biomes: misunderstood, neglected, and under threat, Trends. Ecol. Evol., 29, 205–213, https://doi.org/10.1016/j.tree.2014.02.004, 2014.

Pendrill, F., Persson, U. M., Godar, J., Kastner, T., Moran, D., Schmidt, S., and Wood, R.: Agricultural and forestry trade drives large share of tropical deforestation emissions, Glob. Environ. Chang., 56, 1–10, https://doi.org/10.1016/j.gloenvcha.2019.03.002, 2019.

Peng, S. S., Piao, S. L., Zeng, Z. Z., Ciais, P., Zhou, L. M., Li, L. Z. X., Myneni, R. B., Yin, Y., and Zeng, H.: Afforestation in China cools local land surface temperature, Proc. Natl. Acad. Sci. U.S.A., 111, 2915–2919, https://doi.org/10.1073/pnas.1315126111, 2014.

Pingali, P. L.: Green, Revolution: Impacts, limits, and the path ahead, Proc. Natl. Acad. Sci. U.S.A., 109, 12302–12308, https://doi.org/10.1073/pnas.0912953109, 2012.

Pongratz, J., Raddatz, T., Reick, C. H., Esch, M., and Claussen, M.: Radiative forcing from anthropogenic land cover change since A.D. 800, Geophys. Res. Lett., 36, L02709, https://doi.org/10.1029/2008GL036394, 2009.

Ramanathan, V.: Greenhouse Effect Due to Chlorofluorocarbons: Climatic Implications, Science, 190, 50–52, https://doi.org/10.1126/science.190.4209.50, 1975.

Sherwood, S. C., Bony, S., Boucher, O., Bretherton, C., Forster, P. M., Gregory, J. M., and Stevens, B.: Adjustments in the Forcing-Feedback Framework for Understanding Climate Change, Bull. Amer. Meteor. Soc., 96, 217–228, https://doi.org/10.1175/BAMS-D-13-00167.1, 2015.

Spawn, S. A., Lark, T. J., and Gibbs, H. K.: Carbon emissions from cropland expansion in the United States, Environ. Res. Lett., 14, 045009, https://doi.org/10.1088/1748-9326/ab0399, 2019.

State Forestry Administration of the People's Republic of China Seventh National Forest Resource Inventory Report (2004-2008), (State Forestry Administration of the People's Republic of China, Beijing), 2009.

Stibig, H. J., Achard, F., Carboni, S., Raši, R., and Miettinen, J.: Change in tropical forest cover of Southeast Asia from 1990 to 2010, Biogeosciences, 11, 247–258, https://doi.org/10.5194/bg-11-247-2014, 2014.

Sun, W., Ding, X., Su, J., Mu, X., Zhang, Y., Gao, P., and Zhao, G.: Land use and cover changes on the Loess Plateau: A comparison of six global or national land use and cover datasets, Land Use Policy, 119, 106165, https://doi.org/10.1016/j.landusepol.2022.106165, 2022.

Teluguntla, P. G., Thenkabail, P. S., Xiong, J., Gumma, M. K., Giri, C., Milesi, C., Ozdogan, M., Congalton, R., Tilton, J., Sankey, T. T., Massey, R., Phalke, A., and Yadav, K.: Global Cropland Area Database (GCAD) derived from remote sensing in support of food security in the twenty-fifirst century: Current achievements and future possibilities, In P. S. Thenkabail (Ed.), Remote sensing handbook. Volume II, Land resources monitoring, modeling, and mapping with remote sensing (Chap. 7, p. 849), Chapter 7. Boca Raton: CRC Press, 2015.

Vose, R. S., Kari, T. R., Easterling, D. R., Williams, C. N., and Menne, M. J.: Impact of land-use change on climate, Nature, 427, 213–214, https://doi.org/10.1038/427213b, 2004.

Wang, X. M., Ge, Q. S., Geng, X., Wang, Z. S., Gao, L., Bryan, B. A., Chen, S. Q., Su, Y. N., Cai, D. W., Ye, J. S., Sun, J. M., Lu, H. Y., Liu, B. L., Dong, Z. B., Cao, S. X., Hua, T., Chen, S. Y., Sun, F. B., Luo, G. P., Wang, Z. T., Hu, S., Xu, D. Y., Chen, M. X., Li, D. F., Liu, F., Xu, X. L., Han, D. M., Zheng, Y., Xiao, F. Y., Li, X. B., Wang, P., and Chen, F. H.: Unintended consequences of combating desertification in China, Nat. Commun., 14, 1139, https://doi.org/10.1038/s41467-023-36835-z, 2023.

Ward, D. S., Mahowald, N. M., and Kloster, S.: Potential climate forcing of land use and land cover change, Atmos. Chem. Phys., 14, 12701–12724, https://doi:10.5194/acp-14-12701-2014, 2014.

Winkler, K., Fuchs, R., Rounsevell, M., and Herold, M.: Global land use changes are four times greater than previously estimated, Nat. Commun., 12, 2501, https://doi.org/10.1038/s41467-021-22702-2, 2021.

Yang, J. X.: China's Rapid Urbanization, Science, 342, 310–310, https://doi.org/10.1126/science.342.6156.310-a, 2013.

Zablon, A. A., Paolo, N., Vitaly, Z., and David, W.: Impact of grassland conversion to forest on groundwater recharge in the Nebraska Sand Hills, J. Hydrol. Reg. Stud., 15, 171–183, https://doi.org/10.1016/j.ejrh.2018.01.001, 2018.

Zhang, X. D., Huang, T., Zhang, L. M., Shen, Y. J., Zhao, Y., Gao, H., Mao, X. X., Jia, C. H., and Ma, J. M.: Three-North Shelter Forest Program contribution to long-term increasing trends of biogenic isoprene emissions in northern China, Atmos. Chem. Phys., 16, 6949–6960, https://doi.org/10.5194/acp-16-6949-2016, 2016.

Zhang, X. D., Huang, T., Zhang, L. M., Gao, H., Shen, Y. J., and Ma, J. M.: Trends of deposition fluxes and loadings of sulfur dioxide and nitrogen oxides in the artificial Three Northern Regions Shelter Forest across northern China, Environ. Pollut., 207, 238–247, https://doi.org/10.1016/j.envpol.2015.09.022, 2015.

1163 Zhu, F., Emile-Geay, J., Mckay, N. P., Hakim, G. J., Khider, D., Ault, T. R., Steig, E. J., Dee,
1164   S., and Kirchner, J. W.: Cliamte models can correctly simulate the continuum of global-
1165   average temperature variability, Proc. Natl. Acad. Sci. U.S.A., 116, 8728–8733,
1166   https://doi.org/10.1073/pnas.1809959116, 2019.
1167